Regulating stochastic clocks

Zhe Fei* † Weixuan Xia* ‡

Started 2021 This version: July 4, 2023

Abstract

Stochastic clocks represent a class of time change methods for incorporating trading activity into continuous-time financial models, with the ability to deal with typical asymmetrical and tail risks in financial returns. In this paper we propose a significant improvement of stochastic clocks for the same objective but without decreasing the number of trades or changing the trading intensity. Our methodology targets any Lévy subordinator, or more generally any process of nonnegative independent increments, and is based on various choices of regulating kernels motivated from repeated averaging. By way of a hyperparameter linked to the degree of regulation, arbitrarily large skewness and excess kurtosis of returns can be easily achieved. Generic-time Laplace transforms, characterizing triplets, and cumulants of the regulated clocks and subsequent mixed models are analyzed, serving purposes ranging from statistical estimation and option price calibration to simulation techniques. Under specified jump—diffusion processes and tempered stable processes, a robust moment-based estimation procedure with profile likelihood is developed and a comprehensive empirical study involving S&P500 and Bitcoin daily returns is conducted to demonstrate a series of desirable effects of the proposed methods.

MSC2020 Classifications: 60E07; 60G51; 60H30

JEL Classifications: C13; C65; G12

KEYWORDS: Asymmetrical and tail risks; Lévy subordinators; regulating kernels; tempered stable processes; moment-based estimation; profile likelihood

1 Introduction

Financial returns have long been documented to have excessive skewness and kurtosis relative to those of an (un)conditional Gaussian distribution, leading to asymmetrical and tail risks; see, among others, [Bollerslev, 1987] [16], [Mittnik et al., 2000] [49], [Jondeau and Rockinger, 2003] [35], and [Ornthanalai, 2014] [51]. This phenomenon appears to be even more salient in the recently burgeoning cryptocurrency market which exhibits very high volatility due to its heavy reliance on supply and demand and market attention; see [Troster et al., 2019] [63], [Gkillas and Katsiampa,

^{*}Department of Finance, Boston University Questrom School of Business, Boston, MA, USA.

[†]Email: <u>zhefei@bu.edu</u>

[‡]Corresponding author. Email: gabxia@bu.edu

2018] [30], [Chaim and Laurini, 2019] [20], and [Liu and Tsyvinski, 2021] [42], e.g., for the major cryptocurrencies including Bitcoin.

In continuous-time modeling, a well-known method for incorporating distributional asymmetry and heavy tails is to replace the usual, constantly forward-moving clock under which the underlying stochastic process is monitored with a generally independent nondecreasing stochastic process. The latter process is termed a "stochastic clock" and can be linked to trading volumes or the number of trades (see [Clark, 1973] [23], [Ané and Geman, 2000] [5], [Geman et al., 2001] [29], and [Geman, 2008] [28]). Stemming from the celebrated Dambis–Dubins–Schwarz theorem of time change, [Monroe, 1978] [50] first gave the possibility to represent any semimartingale as a time-changed Brownian motion. When the stochastic clock is modeled by a nonnegative process with independent and stationary increments, namely a Lévy subordinator, such a representation has had striking consequences in generating a variety of purely discontinuous Lévy processes as mixed models, which have flourished for the last two decades in time series econometrics, option pricing, and portfolio management, some recent contributions including [Madan et al., 2019] [47], [Aguilar et al., 2020] [2], and [Fallahgoul and Loeper, 2021] [27].

The key idea behind using stochastic clocks in the absence of a drift component in producing large skewness and kurtosis is rather comprehensible: Pure-jump stochastic clocks progress in a staircase-like manner and are less active – and less uniform – than the usual "sloped" clock of calendar time, and hence possess relatively slower local speed, representing trading activity that does not take place in a perfectly continuous manner, which enables them to adequately tell apart periods of intensive trading and other relatively calmer ones. Perhaps the two most predominant clocks of this type are the gamma process and the inverse Gaussian process, which were studied in [Madan et al., 1998] [46] and [Barndorff-Nielsen, 1997] [7], respectively, to time-change a drifted Brownian motion for building discontinuous models in dealing with skewed and leptokurtic financial returns.¹

Noteworthily, when working with ordinary stochastic clocks under Lévy subordinators, the asymmetrical and tail risks of returns are largely controlled by the number of trades occurring for a significant period of time (i.e., the aggregate level of trading activity) through an infinitedivisibility (i.e., time-multiplicative) parameter (as mentioned in the overview in [Schoutens, 2003, Chap. 4] [59]), or the long-term trading intensity (equivalently, the variation of trading volumes) via an α -stability index (in the case of the stable family; see [Samorodnitsky and Taggu, 1994] [57] e.g.). More specifically, the matching of a high empirical kurtosis level will require decreasing the value of the infinite-divisibility parameter which is a direct measurement of the amount of jumps,² or altering the stability index which is heavily tied to the microstructure or the local regularity of sample paths. Such an operation seems totally innocuous when return distributions are analyzed statically, after imposing assumptions of i.i.d. samples. However, in reality, the aggregate number of trades cannot be expected to be unlimitedly small, or close to zero, leading effectively to degeneracy, or trading halts; on the other hand, the long-term trading intensity is generally specified a priori without being optimized and may be estimated in a dynamical fashion using techniques of empirical power variations (see, e.g., [Aït-Sahalia and Jacod, 2009] [3], [Todorov and Tauchen, 2011] [62], [Jing et al., 2012] [34], and [Todorov, 2021] [61]), which of course varies with the frequencies at which data are observed. With restrictions on these two important dimensions, nearly

¹The same processes also play an important role in many nonfinancial fields, especially in reliability engineering to model the degradation phenomena of structural components (see the overview by [Ye and Xie, 2015] [70]).

 $^{^2}$ The intuition is that as such a parameter tends to zero in value, the corresponding distribution becomes degenerate.

all the noticed Lévy models will not function well in coping with diverse asymmetrical and tail risks of returns.

In connection with this, we are motivated to consider yet another possibility for the same purpose, by changing the size of local movements of a stochastic clock instead of decreasing their amount or adjusting the corresponding activity level. From the perspective of trading activity, this would mean that the spread of trade sizes may be enlarged at will without having to alter the level of trading intensity or stick to an implausibly small number of trades. In doing so, we prefer to operate in a continuous-time environment because discrete-time analogies are easy to develop subsequently, whereas it will be understandably difficult to go in the opposite direction, e.g., to ensure infinite divisibility in finite dimensions.

Besides, consideration of such a possibility will be beneficial in unraveling the microstructure of returns from low-frequency data via a connection to phenomena that trigger abnormal trading volumes, with ample empirical evidence. For instance, the goal to increase the sparsity of trade size distributions is in agreement with the presence of large speculators in traditional and cryptocurrency markets (mentioning, e.g., [Chang et al., 1997] [21] and [Blau, 2017] [14], respectively) or the prevalence of trade-size clustering (referring to [Alexander and Peterson, 2008] [4] and [Chen, 2019] [22]). In this regard, the linkage between skewed and leptokurtic returns and the theoretical moments of the driving stochastic clock is simply embodied by the famous price-volume relationship (see, e.g., [Karpoff, 1987] [37] and [Richardson and Smith, 1994] [55]).

With the foregoing aspects in mind, in this paper we aim to propose a unified approach towards regulating any existing stochastic clock without impairing important fundamental properties. In this context, the act of "regulating" can be understood in the ordinary sense – a stochastic clock is continually adjusted with the intent of achieving a desirable local speed, making it more reliable for capturing the differences in trading activity over time. As a starting point, however, our methodology is concentrated on the aforesaid Lévy subordinators but will be easily extendable to processes of independent but time-inhomogeneous increments, or Sato processes (see [Sato, 2006] [58] and [Eberlein and Madan, 2009] [26]), all of which can be subsequently applied to build structurally more complex stochastic clocks with mean-reverting acceleration and continuous movements that can deal with volatility clustering (see [Carr and Wu, 2004] [19]). The regulated stochastic clocks have essentially the same functionalities as the originals, and can be used to time-change diffusion processes to spawn multifarious semimartingales with discontinuities, albeit with much larger capacity in dealing with asymmetrical and tail risks.

That being said, our approach can also be exploited to generate a rich class of unexplored Lévy processes comfortable for financial modeling. As expected, this newfound dimension is encoded into a hyperparameter representing the degree of regulation, i.e., how much slower the regulated clock is compared with the unregulated one, and kept as independent as possible from the roles of other shape parameters. The resultant processes are shown to be analytically tractable whether it be statistical estimation or risk-neutral valuation of options that is of interest.

The remainder of this paper is structured as follows. In Section 2 we present our main methodology in three recipes, all of which serve to regulate a stochastic clock to any intended degrees. The effect of clock regulation on the jump behaviors depicting corresponding evolution of trading activity is analyzed (Theorem 1, Theorem 2, and Corollary 1) and the impact on asymmetry and tail heaviness of the original distribution is examined in detail (Corollary 2). Then, we present in Section 3 two simple ways for utilizing the (un)regulated stochastic clocks in order to construct real-valued mixed models. In Section 4, we demonstrate clock regulation on two important spe-

cial cases featuring jump–diffusion models and purely discontinuous models and discuss their potential applications in finance as well as other fields. Section 5 outlines two possible candidates for optimizing the degree of regulation: one employing a robust moment-based estimation procedure combined with profile log-likelihood and the other using option price calibration with numerical Fourier inversion techniques, which underlie our empirical study in Section 6 concerning S&P500 and Bitcoin returns and Bitcoin options. Conclusions are drawn in Section 7 along with a summary of the properties of the three recipes and highlights on future research directions. All mathematical proofs are presented at the end of the paper, in Appendix A.

2 Regulated stochastic clocks

As already noted, we shall develop our methodology using Lévy processes exclusively. By having independent and stationary increments, such processes are easy to manage and sit at the core of statistical estimation with i.i.d. temporal data. To begin with, we outline some basic intuition.

Let $X \equiv (X_t)_{t \geq 0}$ be a Lévy subordinator (nondeterministic by default), acting as a stochastic clock. The objective of regulation lies in properly compressing the amplitude of its moderate jumps (for moderate values the jump component $|\Delta X|$), and an attendant consequence is that the finite-dimensional distribution of X will tend to have greater asymmetry and a heavier right tail, as measured by the skewness and kurtosis. Thus, suppose that $\phi_{X_t}(u) := \mathsf{E} e^{-uX_t}$ is the Laplace transform (LT) of the random variable X_t for generic t > 0, assumed to be definable in a neighborhood of the origin (in \mathbb{C}), and then with the canonical expansion

$$\log \phi_{X_t}(u) = \sum_{m=0}^{\infty} \frac{(-u)^m K_t(m)}{m!}, \quad u \in \mathbb{C}$$
 (2.1)

in terms of corresponding cumulants $K_t(m)$, $m \in \mathbb{N}$ (with $K_t(0) = 0$), the objective is converted to finding, for a fixed u, a linear functional $\mathscr{I}: \mathbb{C}^{\{\alpha u : \alpha \in [0,1]\}} \to \mathbb{C}$ such that, from (2.1),

$$(\mathcal{I}\log\phi_{X_t})(u)=\sum_{m=0}^{\infty}\frac{C_m(-u)^mK_t(m)}{m!},$$

where the time-invariant factors C_m 's satisfy $|C_m| \le 1$ and $C_{m+1} \le C_m$, $\forall m$. These relations will immediately render cumulants of larger (up to four) orders more reduced. Although there are obviously infinitely many possible ways to construct such a functional, \mathscr{I} should be conceptually matched with a recipe operating on the sample paths $[0, t] \ni s \mapsto X_s$ to which the collection $\{\phi_{X_t}^{\alpha}: \alpha \in [0, 1]\}$ of LTs correspond; otherwise temporal structures represented by path properties will be difficult to justify if possible at all. In what follows we are going to present three utterly simple and closely related recipes of this nature, by exploiting continuous temporal averaging.

2.1 Repeated averaging-induction: Three recipes

We design our **first recipe** as follows. Set $\bar{X}^{(0)} := X^{(0)} \equiv X$ and, for any $n \in \mathbb{N}_{++} \equiv \mathbb{N} \setminus \{0\}$, repeatedly define the running averages

$$\bar{X}_0^{(n)} = 0; \quad \bar{X}_t^{(n)} := \frac{1}{t} \int_0^t \bar{X}_s^{(n-1)} ds, \quad t > 0.$$
 (2.1.1)

For each $n \ge 1$, $\bar{X}^{(n)}$ is a stochastic process having P-a.s. continuous sample paths, where continuity at 0 follows by the dominated convergence theorem. More specifically, the sample paths $t \mapsto \bar{X}^{(n)}_t$ belong to the class $\mathscr{C}^{n-1}(\mathbb{R}_+;\mathbb{R}_+)$ of (n-1)th-order differentiable functions for $n \ge 1$, P-a.s., as a result of repeated integration.

Since (2.1.1) operates a linear functional, it is clear that for every $n \ge 1$ and fixed t > 0 the random variable $\bar{X}_t^{(n)}$ has an infinitely divisible distribution, which induces a unique Lévy process that is also nonnegative, which we denote as

$$X_t^{(n)} \stackrel{\text{d.}}{=} \bar{X}_t^{(n)}, \quad t \ge 0, \ n \in \mathbb{N}_{++}.$$
 (2.1.2)

By nonnegativity every $X^{(n)}$ can be used as a different stochastic clock, and will be referred to as the **type-I** regulated X-clock of degree n.

The intuition behind the first recipe is rather clear: Averaging in time has a natural effect of contracting moderate values of the sample paths and continuing to do so will tend to enlarge such an effect. To give some remarks, in the special case n=1, the process $\bar{X}^{(1)}=1/(\cdot)\int_0^{\cdot}X_s\mathrm{d}s$ is precisely the running average of X, which is heavily tied to linear integral functionals of Lévy processes; such integrals have been widely applied to trace the cumulative patterns of various stochastic systems; some notable examples include the total cost of random epidemics (see, e.g., [Downton, 1972] [25] and [Pollett, 2003] [54]), cumulation of count data generalized to non-integer values ([Orsingher and Polito, 2013] [52]) or count data with overdispersion ([Xia, 2019] [67]), and the modeling of structural degradation phenomena in the presence of memory effects (see [Tseng and Peng, 2004] [64] and [Xia, 2021, Sect. 4.1] [68]).

Note that the averaging–induction procedure also works for any integer $n \ge 1$, and hence it is intuitive to consider inducing a Lévy process for each n using (2.1.2), before initiating a subsequent averaging step (2.1.1). In this way the integrand in the averaging step can be made a Lévy process even for $n \ge 2$, and each resultant averaged process will correspond to the linear functional of a certain Lévy process. Such an idea leads to our **second recipe**. Likewise, set $\tilde{X}^{(0)} := Y^{(0)} \equiv X$, and then repeatedly utilize the first recipe for every $n \in \mathbb{N}_{++}$ in the following fashion:

$$\tilde{X}_0^{(n)} = 0; \quad \tilde{X}_t^{(n)} := \frac{1}{t} \int_0^t Y_s^{(n-1)} ds, \quad t > 0,$$
 (2.1.3)

where $Y^{(n)}$'s are induced Lévy processes such that

$$Y_t^{(n)} \stackrel{\mathrm{d.}}{=} \tilde{X}_t^{(n)}, \quad t \ge 0, \ n \in \mathbb{N}_{++}.$$

It is clear that the averaged processes $\bar{X}^{(1)}$ and $\tilde{X}^{(1)}$ are indistinguishable, and so are the induced processes $X^{(1)}$ and $Y^{(1)}$, but for $n \geq 2$ they are different with dissimilar path properties – the sample paths $t \mapsto \tilde{X}_t^{(n)}$ will remain in the class $(\mathscr{C} \setminus \mathscr{C}^1)(\mathbb{R}_+; \mathbb{R}_+)$ (P-a.s.) for $n \geq 2$.

It can be shown (see the proof of Theorem 1 in Appendix A) that the second recipe can be essentially thought to average the log-LT, while in comparison the first recipe, by construction, has the averaging effect on the sample paths. We will refer to the process $Y^{(n)}$, $n \ge 1$, as the **type-II** regulated X-clock of degree n.

In the averaging step (2.1.1), if we stack up the time scale (1/t) outside of the integral operators for every $n \ge 2$, the averaging procedure becomes a folded cumulation with a one-time power scaling, and we shall have our **third recipe**. Set $\check{X}^{(0)} := Z^{(0)} \equiv X$ and define the quasi-averages

$$\check{X}_0^{(n)} = 0; \quad \check{X}_t^{(n)} := \frac{1}{t^n} \underbrace{\int \cdots \int_0^t X_s \underbrace{\mathrm{d}s \cdots \mathrm{d}s}_n}_{n}, \quad t > 0, \ n \in \mathbb{N}_{++}, \tag{2.1.4}$$

which has an infinitely divisible distribution for the same reason as in (2.1.1), and induce a unique nonnegative Lévy process,

$$Z_t^{(n)} \stackrel{\mathrm{d.}}{=} \breve{X}_t^{(n)}, \quad t \ge 0, \ n \in \mathbb{N}_{++},$$

referred to as the **type-III** regulated X-clock of degree n.

It is obvious that the processes $\check{X}^{(n)}$ and $\bar{X}^{(n)}$ have the same degree of path smoothness but are guaranteed to coincide (up to indistinguishability) only if n=1. Besides, the distribution of $\check{X}_t^{(n)}$ is also infinitely divisible for every $n \ge 1$ and fixed t.

We present some general formulae for the LTs of the three types of regulated stochastic clocks in Theorem 1, which are naturally extended to non-integer-valued n > 0 as well. This aspect hints at the extension of the three recipes to the sense of averaging of fractional degrees and will be considered in the optimization of the regulation degree n.

Theorem 1. For generic t > 0 and any n > 0, the LTs of $\bar{X}_t^{(n)}$, $\tilde{X}_t^{(n)}$, and $\check{X}_t^{(n)}$, are given by

$$\phi_{\bar{X}_{t}^{(n)}}(u) := Ee^{-u\bar{X}_{t}^{(n)}} = \exp\left(t\int_{0}^{1}\log\phi_{X_{1}}\left(\left(1 - \frac{\Gamma(n, -\log s)}{\Gamma(n)}\right)u\right)ds\right),
\phi_{\bar{X}_{t}^{(n)}}(u) := Ee^{-u\bar{X}_{t}^{(n)}} = \exp\left(\frac{t}{\Gamma(n)}\int_{0}^{1}(-\log v)^{n-1}\log\phi_{X_{1}}(uv)dv\right),
\phi_{\bar{X}_{t}^{(n)}}(u) := Ee^{-u\bar{X}_{t}^{(n)}} = \exp\left(t\int_{0}^{1}\log\phi_{X_{1}}\left(\frac{s^{n}u}{\Gamma(n+1)}\right)ds\right), \quad \text{Re}\, u \ge 0,$$
(2.1.5)

respectively, where $\Gamma(\cdot)$ and $\Gamma(\cdot,\cdot)$ symbolize, respectively, the usual gamma function and the (upper) incomplete gamma function.

In any case, the recipes have given rise to three families of stochastic clocks, controlled by the degree n of regulation. The effect of operating the three recipes on the unregulated clock X is twofold – on path properties and distributional properties, as we are bound to investigate next.

2.2 Characterizing triplets

From their primary motivation, the three recipes are all supposed to compress the jumps of X into extreme values. To confirm such effects, it is necessary to derive the characterizing triplets of the regulated clocks $X^{(n)}$'s, $Y^{(n)}$'s, and $Z^{(n)}$'s governing their sample path properties. Doing so will also be helpful for developing simulation methods, the main reason being that the LTs that we have obtained in (2.1.5), having exponentiated integrals, are generally difficult to invert analytically, thus circumventing the implementation of inverse sampling methods.

First, there is no Brownian component in $X^{(n)}$'s, $Y^{(n)}$'s or $Z^{(n)}$'s and we assume without loss of generality that there is no drift as well, so that we can concentrate on the corresponding Lévy measure. More specifically, suppose that the LT ϕ_{X_1} takes the following general form due to the Lévy–Khintchine representation:

$$\phi_{X_1}(u) = \exp \int_0^\infty (e^{-uz} - 1)\nu(\mathrm{d}z), \quad \mathrm{Re}\, u \ge 0,$$

with the characterizing triplet (0,0,v), for some Lévy measure³ v imposed on $\mathcal{B}(\mathbb{R}_+)$ such that $v(\{0\}) = 0$ and $\int_0^\infty (z \wedge 1) v(\mathrm{d}z) < \infty$. Then, the characterizing triplets of $X^{(n)}$, $Y^{(n)}$, and $Z^{(n)}$, given

 $^{^3}$ The notation v_X will occasionally be used for the Lévy measure of X in the mathematical proofs (Appendix A) to avoid ambiguity.

n>0, are denoted as $(0,0,\tilde{v}^{(n)})$, $(0,0,\tilde{v}^{(n)})$, and $(0,0,\tilde{v}^{(n)})$ respectively, which make the representations

$$\phi_{\tilde{X}_{1}^{(n)}}(u) = \exp \int_{0}^{\infty} (e^{-uz} - 1)\tilde{v}^{(n)}(dz),$$

$$\phi_{\tilde{X}_{1}^{(n)}}(u) = \exp \int_{0}^{\infty} (e^{-uz} - 1)\tilde{v}^{(n)}(dz),$$

$$\phi_{\tilde{X}_{1}^{(n)}}(u) = \exp \int_{0}^{\infty} (e^{-uz} - 1)\tilde{v}^{(n)}(dz).$$
(2.2.1)

Theorem 2. For any n > 0, we have

$$\bar{v}^{(n)}(dz) = \Gamma(n) \int_{1}^{\infty} \frac{v(d(yz))}{y^{2}Q^{n-1}(n, 1-1/y)} dy,
\bar{v}^{(n)}(dz) = \frac{1}{\Gamma(n)} \int_{1}^{\infty} \frac{(\log y)^{n-1}v(d(yz))}{y^{2}} dy,
\bar{v}^{(n)}(dz) = \int_{\Gamma(n+1)}^{\infty} \left(\frac{\Gamma(n+1)}{y}\right)^{1/n} \frac{v(d(yz))}{ny} dy, \quad z \ge 0,$$
(2.2.2)

where Q(n, s) is the inverse regularized (upper) incomplete gamma function.⁴

Furthermore, if v is absolutely continuous with respect to Lebesgue measure, then

$$\bar{\ell}^{(n)}(z) := \frac{\bar{v}^{(n)}(dz)}{dz} = \Gamma(n) \int_{1}^{\infty} \frac{\ell(yz)}{yQ^{n-1}(n, 1 - 1/y)} dy,
\bar{\ell}^{(n)}(z) := \frac{\tilde{v}^{(n)}(dz)}{dz} = \frac{1}{\Gamma(n)} \int_{1}^{\infty} \frac{(\log y)^{n-1} \ell(yz)}{y} dy,
\bar{\ell}^{(n)}(z) := \frac{\tilde{v}^{(n)}(dz)}{dz} = \int_{\Gamma(n+1)}^{\infty} \left(\frac{\Gamma(n+1)}{y}\right)^{1/n} \frac{\ell(yz)}{n} dy, \quad z \ge 0,$$
(2.2.3)

with $v(dz) = \ell(z)dz$.

We remark that the Lévy measures $\tilde{v}^{(n)}$'s, $\tilde{v}^{(n)}$'s, and $\check{v}^{(n)}$'s from (2.2.2), for $n \ge 1$, are all absolutely continuous because of integration, and thus their associated Lévy densities on the left-hand side of (2.2.3) exist unconditionally. More importantly, we have the following equalities among their Blumenthal–Getoor indices ([Blumenthal and Getoor, 1961] [15]).

Corollary 1. For any n > 0, it holds that

$$\mathfrak{B}(X^{(n)}) := \inf \left\{ p > 0 : \int_0^1 |z|^p \bar{v}^{(n)}(\mathrm{d}z) < \infty \right\} = \mathfrak{B}(X), \tag{2.2.4}$$

and similarly $\mathfrak{B}(Y^{(n)}) = \mathfrak{B}(Z^{(n)}) = \mathfrak{B}(X)$.

Corollary 1 means that none of the three recipes alters the path regularity of X, which is beyond doubt a very desirable property as there is never an intention of changing the jump activity of the underlying models connected with trading intensities (recalling Section 1). On the other hand, all

⁴It is understood as the unique solution $x \ge 0$ to the transcendental equation $\Gamma(n,x)/\Gamma(n) = s$ for $s \in [0,1)$; see [DiDonato and Morris, 1986] [24].

of the induced Lévy measures govern jumps of arbitrarily large amplitudes, whereas their actual weights (namely likelihood) will depend on the functional form of v (or that of the LT), subject to further adjustment of its parameters, and through the foregoing relations. This aspect will be clearer as we move to specific distribution families of interest in Section 4.

To gain additional insight into how the three recipes distort the Lévy measures $\bar{v}^{(n)}$, $\tilde{v}^{(n)}$, and $\tilde{v}^{(n)}$ from a comparative angle, it is first observed from (2.2.2) in Theorem 2 that these Lévy measures do coincide if and only if n=1. Upon the substitution $yz\mapsto y$, they can be viewed as fractional integrals of the Lévy measure v of X under different kernels, which with y=1 fixed boil down to the functions $\Gamma(n)/Q^{n-1}(n,1-z)$, $(-\log z)^{n-1}/\Gamma(n)$, and $z^{1/n-1}/n$, respectively, defined for $z\in(0,1)$. Interestingly, we then observe that the first two functions are precisely the derivatives in magnitude of $e^{-Q(n,1-z)}$ and $1-\Gamma(n,-\log z)/\Gamma(n)$, respectively, which happen to be inverses of each other. Put differently, the effects on the (average-induced) Lévy measures from the first two recipes are perfectly complementary, in the sense that neither dominates the other. Differently, the third function integrates in magnitude to $1-z^{1/n}$, which is not in direct comparison with the others, for the third recipe, strictly speaking, does not embody a running average for $n \neq 1$. This discussion is further illustrated in Figure 1, with five integer degrees $n \in \mathbb{N} \cap [1,5]$ of regulation. We see that the first recipe, which averages the sample paths, has a larger impact (distortion) when v is concentrated on small values of \mathbb{R}_+ , relative to the second, which at bottom averages the log-LT. In addition, the larger the regulation degree, the faster the impact differences are reflected.

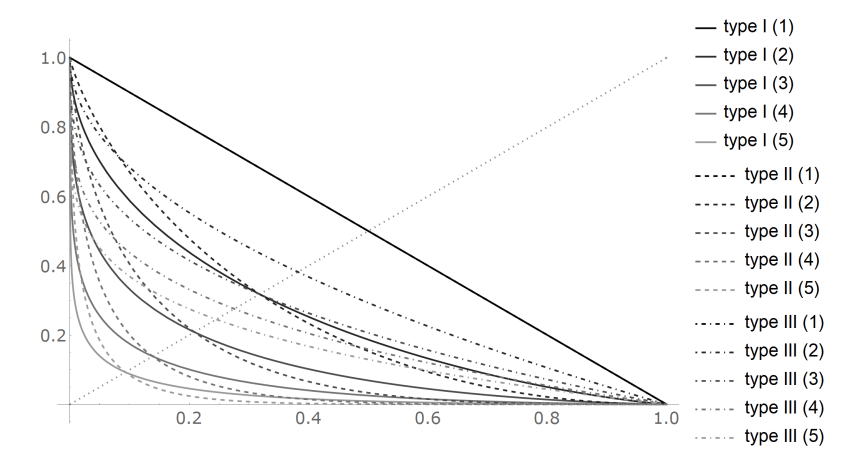


Figure 1: Regulation impact on induced Lévy measures

2.3 Asymmetry and tail heaviness

The static effect from operating the three recipes is to enlarge the asymmetry and (right) tail heaviness of the distribution of the unregulated clock X_t for any fixed t > 0. With the LTs in (2.1.5) at hand, computation of the statistics of the corresponding regulated clocks $X_t^{(n)}$'s and $Y_t^{(n)}$'s is straightforward. More particularly, we shall focus on the impact of regulation on skewness and excess kurtosis. Let us restate from (2.1) that the corresponding cumulants are defined to be the series coefficients $\{\bar{K}_t(m)\}_{m=0}^{\infty}$ and $\{\tilde{K}_t(m)\}_{m=0}^{\infty}$ in

$$\log \phi_{\bar{X}_t}(u) = \sum_{m=0}^{\infty} \frac{(-u)^m \bar{K}_t(m)}{m!}, \quad \log \phi_{\bar{X}_t}(u) = \sum_{m=0}^{\infty} \frac{(-u)^m \tilde{K}_t(m)}{m!}, \quad \log \phi_{\bar{X}_t}(u) = \sum_{m=0}^{\infty} \frac{(-u)^m \bar{K}_t(m)}{m!},$$

with $\bar{K}_t(0) = \tilde{K}_t(0) = 0$. The next corollary explains how the cumulants vary with the regulation degree n.

Corollary 2. For any n > 0, we have the cumulant reduction relations

$$\bar{K}_{t}^{(n)}(m) = C_{m,n}K_{t}(m), \quad \tilde{K}_{t}^{(n)}(m) = \frac{K_{t}(m)}{(m+1)^{n}}, \quad \check{K}_{t}^{(n)}(m) = \frac{K_{t}(m)}{(mn+1)\Gamma^{m}(n+1)}, \tag{2.3.1}$$

with the sequence

$$C_{m,n} = \int_0^1 \left(1 - \frac{\Gamma(n, -\log s)}{\Gamma(n)}\right)^m \mathrm{d}s, \quad m \in \mathbb{N}_{++}, \tag{2.3.2}$$

which is rational for $n \in \mathbb{N}_{++}$.

Using Corollary 2, the relations for the mean, variance, skewness and excess kurtosis of the type-I *n*-degree regulated *X*-clocks are given by

$$\begin{split} \mathsf{E} X_t^{(n)} &= C_{1,n} \mathsf{E} X_t, \quad \mathsf{Var} X_t^{(n)} = C_{2,n} \mathsf{Var} X_t, \\ \mathsf{Skew} X_t^{(n)} &= \frac{C_{3,n}}{C_{2,n}^{3/2}} \mathsf{Skew} X_t, \quad \mathsf{EKurt} X_t^{(n)} = \frac{C_{4,n}}{C_{2,n}^2} \mathsf{EKurt} X_t. \end{split} \tag{2.3.3}$$

Since the integrand in (2.3.2) admits the series representation ([Abramowitz and Stegun, 1972, Eq. 6.5.29] [1])

$$1 - \frac{\Gamma(n, -\log s)}{\Gamma(n)} = \frac{s(-\log s)^n}{\Gamma(n)} \sum_{k=0}^{\infty} \frac{(-\log s)^k}{(n)_{k+1}} = \frac{s(-\log s)^n}{\Gamma(n+1)} (1 + O(n^{-1})), \text{ as } n \to \infty,$$

carrying out the integral over $s \in (0,1)$ gives

$$C_{m,n} = O\left(n^{(1-m)/2} \left(\frac{m}{m+1}\right)^{mn}\right), \text{ as } n \to \infty,$$
 (2.3.4)

and hence the sequence decays exponentially as n increases for m=1 and (strictly) faster for $m \ge 2$. This indicates that the first recipe shrinks the cumulants of X with acceleration – more aggressively so as regulation continues with n. Note that for m=1 the exponential decay is in fact an equality $C_{1,n}=2^{-n}$. Looking at (2.3.3) and (2.3.4) we can also claim that the type-I regulated clocks have at least exponentially decaying mean and variance but faster-than-exponentially increasing skewness and excess kurtosis, with respect to the degree n of regulation, other things (e.g., parameter values) held equal.

In the case of the type-II regulated clocks, the counterpart of (2.3.3) for $Y_t^{(n)}$ is

$$\mathsf{E} Y_t^{(n)} = \frac{1}{2^n} \mathsf{E} X_t, \quad \mathsf{Var} Y_t^{(n)} = \frac{1}{3^n} \mathsf{Var} X_t, \quad \mathsf{Skew} Y_t^{(n)} = \left(\frac{3\sqrt{3}}{4}\right)^n \mathsf{Skew} X_t, \quad \mathsf{EKurt} Y_t^{(n)} = \left(\frac{9}{5}\right)^n \mathsf{EKurt} X_t. \tag{2.3.5}$$

Intuitively, this signifies that the cumulant-reduction effect of the second recipe is uniform, in the sense that for each additional round of regulation, the mean and variance are reduced by fixed proportions (1/2 and 1/3, respectively) while the skewness and excess kurtosis are simultaneously enlarged by fixed proportions ($3\sqrt{3}/4$ and 9/5, respectively). In consequence, for the type-II regulated *X*-clocks the mean and variance decay exactly exponentially and so do the skewness and excess kurtosis increase, other things equal.

As for the type III, we have similarly from Corollary 2 the quotient $\check{K}_t^{(n)}(m)/K_t(m) = 1/((mn+1)\Gamma^m(n+1))$, $m \in \mathbb{N}_{++}$, and subsequently the following moment relations for $Z_t^{(n)}$:

$$EZ_{t}^{(n)} = \frac{1}{\Gamma(n+2)} EX_{t}, \quad \text{Var} Z_{t}^{(n)} = \frac{1}{(2n+1)\Gamma^{2}(n+1)} \text{Var} X_{t},$$

$$Skew Z_{t}^{(n)} = \frac{(2n+1)^{3/2}}{3n+1} Skew X_{t}, \quad EKurt Z_{t}^{(n)} = \frac{(2n+1)^{2}}{4n+1} EKurt X_{t}. \tag{2.3.6}$$

Upon comparing the above quotient with (2.3.4), with $\Gamma(n+1) = O(\sqrt{n}(n/e)^n)$ as $n \to \infty$ it is seen that the third recipe generates an even severer cumulant-reduction effect than the first recipe does. However, the skewness and excess kurtosis are enlarged with deceleration, noted that $(2n+1)^{3/2}/(3n+1) = O(n^{1/2})$ and $(2n+1)^2/(4n+1) = O(n)$, as $n \to \infty$. Put together, the type-III regulated X-clocks have mean and variance of faster-than-exponential decay whereas the skewness and excess kurtosis exhibit slower-than-linear growth, which properties are in stark contrast with those of the first two types.

On paper, if we do not alter the parameter (if any) values of X, then all three recipes are able to effectively enlarge the asymmetry and tail heaviness of its distribution, with the first having the most significant effect, whereas the downside is that the mean and variance are reduced at the same time. The latter effect is, of course, undesirable for applications, and eluding it will require at least two independent parameters so that the mean and variance can be held constant across the regulation degree n. More specifically, when a real-valued model is to be constructed from X (see Section 3), with the aid of an additional location parameter the mean can be readily fixed by way of centralization, and so the other parameter will most likely (and ideally) be a scale parameter, to which the standard deviation is proportional and the skewness and excess kurtosis are immune. Such a requirement becomes rather standard in statistical inference, and in consequence the skewness and excess kurtosis relations stated in (2.3.3), (2.3.5), and (2.3.6) provide useful implications. We remark, however, that if the mean is to be kept invariant to regulation by way of a shape parameter of X (oftentimes existent for one-sided distributions) then changing its value is likely to enlarge skewness and excess kurtosis at rates different from those in (2.3.3) and (2.3.5), despite exponential growth rates. Such a situation cannot be analyzed from a universal viewpoint and will again depend on the functional form of the LT ϕ_{X_1} , with respect to the shape parameter. More details are provided in Section 4.

Similarly, the results for the statistics stated in this section can be naturally extended for fractional degrees n>0 of regulation. In Figure 2 we give a joint plot of the enlargement effect on asymmetry and tail heaviness for the two recipes with real regulation degrees $n \in (0,5]$, by using (2.3.3), (2.3.5), and (2.3.6) in sequence.

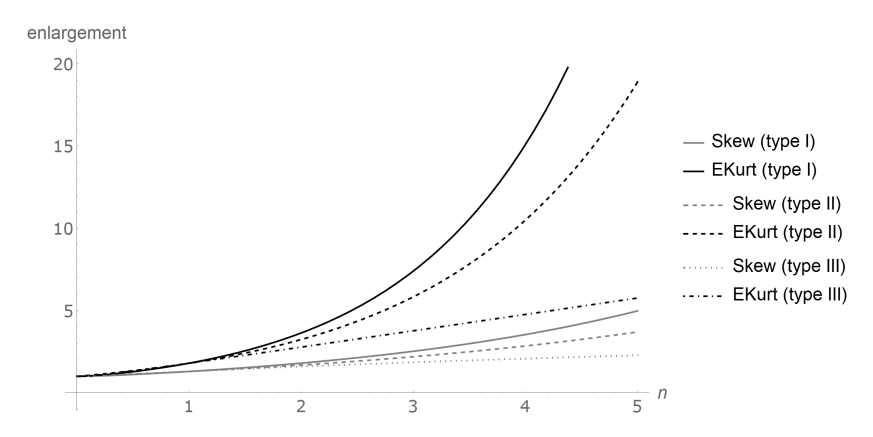


Figure 2: Enlargement effect on asymmetry and tail heaviness with respect to regulation degree

3 Time-changed processes

As aforementioned, the functionality of the regulated clocks $X^{(n)}$'s, $Y^{(n)}$'s, and $Z^{(n)}$'s is meant to be the same as that of X – mathematically, to adjust the time underlying a (continuous) base process and generate a wide class of models for real-valued temporal data such as financial returns. In the following we shall consider two well-known base processes for the mixture, which are also shown to retain, leastways in part, the enlargement effect on asymmetry and tail heaviness through the clock regulation.

3.1 Constant mixtures

The simplest base process is beyond doubt a (deterministic) drift (t) up to positive scaling, and time-changing it by the clock X gives none but X itself. Then, in order to create a real-valued random variable from X it suffices to take the difference of two of its independent copies. Specifically, let X' be an independent copy of X, and then define the difference process

$$\xi_t^X = \mu t + \kappa_1 X_t - \kappa_2 X_t', \quad t \ge 0, \tag{3.1.1}$$

where $\mu \in \mathbb{R}$ is a location parameter and $\kappa_1, \kappa_2 \ge 0$ are additional scale parameters. Then ξ^X is a purely discontinuous real-valued Lévy process admitting the LT (fixing t > 0)

$$\phi_{\xi_t^X}(u) := \mathsf{E} e^{-u\xi_t^X} = e^{-\mu t u} \phi_{X_t}(\kappa_1 u) \phi_{X_t}(-\kappa_2 u), \quad u \in i\mathbb{R},$$
 (3.1.2)

where the domain of Reu can be extended to a neighborhood of 0 provided that (2.1) holds.

Note that since the integral operator $1/t\int_0^t \mathrm{d}s$ is for every t>0 a linear isometry over the space $\mathbb{L}^\infty(\mathbb{R}_+;\mathbb{R}_+)$ of bounded functions, considering such independent differences under the n-degree regulated clocks is no different from operating the three recipes on the initial difference process ξ^X . As a result, we can define the corresponding difference processes under each $X^{(n)}$, $Y^{(n)}$, and $Z^{(n)}$, denoted $\xi^{(n),X}$, $\xi^{(n),Y}$, and $\xi^{(n),Z}$, respectively, in the same way as in (3.1.1).

Corollary 3. For generic t > 0 and any n > 0, the LTs of the constant mixtures subject to clock regulation are given by

$$\begin{split} \phi_{\xi_{t}^{(n),X}}(u) &= e^{-\mu t u} \phi_{\tilde{X}_{t}^{(n)}}(\kappa_{1} u) \phi_{\tilde{X}_{t}^{(n)}}(-\kappa_{2} u), \\ \phi_{\xi_{t}^{(n),Y}}(u) &= e^{-\mu t u} \phi_{\tilde{X}_{t}^{(n)}}(\kappa_{1} u) \phi_{\tilde{X}_{t}^{(n)}}(-\kappa_{2} u), \\ \phi_{\xi_{t}^{(n),Z}}(u) &= e^{-\mu t u} \phi_{\tilde{X}_{t}^{(n)}}(\kappa_{1} u) \phi_{\tilde{X}_{t}^{(n)}}(-\kappa_{2} u), \quad u \in i\mathbb{R}. \end{split}$$
(3.1.3)

Besides, by independence the mth cumulant of $\xi_t^{(n),X}$ for fixed t>0 is nothing but $\mu t \mathbb{I}_{\{1\}}(m) + (\kappa_1^m + (-\kappa_2)^m) \bar{K}_t^{(n)}(m)$ and similarly for $\xi_t^{(n),Y}$ and $\xi_t^{(n),Z}$. If the mean and variance of $\xi_t^{(n),X}$ and $\xi_t^{(n),Y}$ are kept constant by adjusting, respectively, the location parameter μ and a scale parameter of X, then the skewness and excess kurtosis increase at precisely the same rates as those of X stated in (2.3.3), (2.3.5), and (2.3.6), respectively. Therefore, the constant mixture approach also preserves enlargement effects on asymmetry and tail heaviness of the constituent subordinator X, regardless of the additional parameters μ , κ_1 , and κ_2 .

Simplicity notwithstanding, a major drawback of this approach, due to linearity, is that it inevitably inherits the path regularity of X into the processes $\xi^{(n),X}$'s, $\xi^{(n),Y}$'s, and $\xi^{(n),Z}$'s, as the next corollary shows.

Corollary 4. For any
$$n > 0$$
, we have $\mathfrak{B}(\xi^{(n),X}) = \mathfrak{B}(\xi^{(n),Y}) = \mathfrak{B}(\xi^{(n),Z}) = \mathfrak{B}(\xi^X) = \mathfrak{B}(X)$.

However, in some situations, e.g., as mentioned in [Todorov and Tauchen, 2011] [62], a suitable model needs to have sample paths of infinite variation. This is clearly not possible via (3.1.1), because by nonnegativity $\mathfrak{B}(X) \in [0,1)$, thus leading us to consider a second approach.

3.2 Gaussian mixtures

Alternatively, one can construct a real-valued random variable by using it as a scale parameter for an independent Gaussian random variable – a technique called "Gaussian mixture," which is implemented here by way of using X to time-change a Brownian motion with drift (see, e.g., [Barndorff-Nielsen, 1997, Sect. 3.1] [7] and [Madan et al., 1998, Sect. 2] [46]). To be precise, let W be a standard Brownian motion independent of X, and define the mixed process

$$\Xi_t^X = \mu t + \theta X_t + W_{X_t}, \quad t \ge 0,$$
 (3.2.1)

where $\mu \in \mathbb{R}$ is a location parameter and $\theta \in \mathbb{R}$ is a Brownian drift parameter representing signed random momenta. The dispersion of the Brownian motion can be fixed at 1 for simplicity as long as X has a scale parameter, which is already able to capture jump volatility. Then, Ξ^X is also a purely discontinuous real-valued Lévy process. Upon applying the tower property of conditional expectations, the LT of Ξ^X_t for fixed t > 0 is found to be

$$\phi_{\Xi_t^X}(u) := \mathsf{E} e^{-u\Xi_t^X} = e^{-\mu t u} \phi_{X_t} \Big(\theta u - \frac{u^2}{2} \Big), \quad u \in i\mathbb{R}.$$
(3.2.2)

Again, a partial domain extension into $\mathbb{C} \setminus (i\mathbb{R})$ is possible with (2.1).

In a similar fashion, we can time-change the Brownian motion with drift by the regulated clocks, though this would not be equivalent to operating the two recipes on Ξ^X . The resultant processes are denoted as, respectively, $\Xi^{(n),X}$, $\Xi^{(n),Y}$, and $\Xi^{(n),Z}$, with the LTs (t>0) states as follows.

Corollary 5. For generic t > 0 and any n > 0, the LTs of the Gaussian mixtures subject to clock regulation are given by

$$\phi_{\Xi_{t}^{(n),X}}(u) = e^{-\mu t u} \phi_{\tilde{X}_{t}^{(n)}} \left(\theta u - \frac{u^{2}}{2} \right),
\phi_{\Xi_{t}^{(n),Y}}(u) = e^{-\mu t u} \phi_{\tilde{X}_{t}^{(n)}} \left(\theta u - \frac{u^{2}}{2} \right),
\phi_{\Xi_{t}^{(n),Z}}(u) = e^{-\mu t u} \phi_{\tilde{X}_{t}^{(n)}} \left(\theta u - \frac{u^{2}}{2} \right), \quad u \in i\mathbb{R}.$$
(3.2.3)

From Corollary 5, an application of Faà di Bruno's formula yields the cumulants of $\Xi_t^{(n),X}$ in terms the finite sums

$$(-1)^m \frac{\mathrm{d}^m}{\mathrm{d}u^m} \log \phi_{\Xi_t^{(n),X}}(u) \Big|_{u=0} = \mu t \mathbb{1}_{\{1\}}(m) + \sum_{k=1}^m \mathrm{B}_{m,k}(\theta,1) \bar{K}_t^{(n)}(k), \quad m \in \mathbb{N}_{++},$$

where $B_{m,k}(\theta,1)$'s are partial Bell polynomials. In particular, by the order of $m \in \{1,2,3,4\}$ the first four cumulants are: $\mu t + \theta \bar{K}_t^{(n)}(1)$, $\bar{K}_t^{(n)}(1) + \theta^2 \bar{K}_t^{(n)}(2)$, $3\theta \bar{K}_t^{(n)}(2) + \theta^3 \bar{K}_t^{(n)}(3)$, and $3\bar{K}_t^{(n)}(2) + \theta^2 \bar{K}_t^{(n)}(3) + \theta^4 \bar{K}_t^{(n)}(4)$, in order. Similar results hold for $\Xi^{(n),Y}$ and $\Xi^{(n),Z}$. Notably, the elegance of the Gaussian mixture (3.2.1) lies in that the additional parameter θ in its own right acts as a scaling factor on X, so that scaling Ξ^X is fundamentally linked to doing X, making it a feasible task to control the variance of $\Xi^{(n),X}$ (and that of $\Xi^{(n),Y}$ and $\Xi^{(n),Z}$) to be invariant to clock regulation, while the invariance of the mean is taken care of by the location parameter μ . The consequence is that the skewness and kurtosis relations in (2.3.3), (2.3.5), and (2.3.6) set the upper bounds for those (lower-bounded by 1) of the Gaussian-mixed processes, whose exact rates of increase are subject to the value of θ .

The main reason to consider Gaussian mixtures is that they allow for processes with infinite-variation sample paths. Indeed, it can be shown (see Appendix A) that the Blumenthal-Getoor indices of the Gaussian mixtures are precisely double that of X.

Corollary 6. For any
$$n > 0$$
 we have $\mathfrak{B}\left(\Xi^{(n),X}\right) = \mathfrak{B}\left(\Xi^{(n),Y}\right) = \mathfrak{B}\left(\Xi^{(n),Z}\right) = \mathfrak{B}\left(\Xi^{X}\right) = 2\mathfrak{B}(X)$.

Therefore, as long as $\mathfrak{B}(X) \geq 1/2$, Ξ^X , and hence $\Xi^{(n),X}$, $\Xi^{(n),Y}$, and $\Xi^{(n),Z}$, n > 0, on the regulated clocks, will all have jumps of infinite variation. The same idea goes for the Gaussian mixtures on the regulated clocks. This property overcomes the limitation of the constant mixtures and is particularly attractive when flexibility to include highly active jumps in asset returns is required for model formulation.

4 Some important special cases

We now consider two specific distributions of the unregulated clock X for practical interests. By infinite divisibility we fix time at t = 1 unless otherwise specified. Explicit formulae will be presented for the distributions of all three types of regulated clocks, as well as their time-changed processes.

4.1 Poisson process

Let the LT of X_1 be given by $\phi_{X_1}(u) = \exp(\lambda(e^{-u} - 1))$ with shape parameter $\lambda > 0$ (Poisson intensity). Then we have the following specialized formulae.

Proposition 1. If X is a Poisson process with intensity λ , then for any n > 0,

$$\begin{split} \phi_{\tilde{X}_{1}^{(n)}}(u) &= \exp\left(\lambda \left(\Gamma(n) \int_{0}^{1} \frac{e^{-uz}}{\mathbf{Q}^{n-1}(n,1-z)} \mathrm{d}z - 1\right)\right), \\ \phi_{\tilde{X}_{1}^{(n)}}(u) &= \exp\left(\frac{1}{\Gamma(n)} \int_{0}^{1} (-\log v)^{n-1} (e^{-uv} - 1) \mathrm{d}v\right) \stackrel{n \in \mathbb{N}_{++}}{=} \exp(\lambda (\,_{n} \mathbf{F}_{n}(1, \dots, 1; 2, \dots, 2; -u) - 1)), \\ \phi_{\tilde{X}_{1}^{(n)}}(u) &= \exp\left(\lambda \left(\left(\frac{\Gamma(n+1)}{u}\right)^{1/n} \frac{\Gamma(1/n) - \Gamma(1/n, u/\Gamma(n+1))}{n} - 1\right)\right), \quad u \in \mathbb{C}, \end{split}$$
(4.1.1)

where $.F.(\cdots; \cdots; \cdot)$ denotes the generalized hypergeometric function (see [Slater, 1966] [60]); also,

$$\bar{\ell}^{(n)}(z) = \frac{\lambda \Gamma(n) \mathbb{I}_{(0,1]}(z)}{Q^{n-1}(n, 1-z)},$$

$$\tilde{\ell}^{(n)}(z) = \frac{\lambda (-\log z)^{n-1} \mathbb{I}_{(0,1]}(z)}{\Gamma(n)},$$

$$\tilde{\ell}^{(n)}(z) = \frac{\lambda (\Gamma(n+1)z)^{1/n} \mathbb{I}_{(0,1/\Gamma(n+1)]}(z)}{nz}, \quad z > 0.$$
(4.1.2)

It is an easy implication from Proposition 1 that the type-I regulated clock $X^{(n)}$ is of compound Poisson type: In light of the discussion in Subsection 2.2 and with inverse sampling in mind,

$$X_{t}^{(n)} \stackrel{\text{d.}}{=} \sum_{k=1}^{X_{t}} \left(1 - \frac{\Gamma(n, -\log U_{k})}{\Gamma(n)} \right), \quad t \ge 0,$$
(4.1.3)

where $\{U_k\}_{k=1}^{\infty}$ is a sequence of i.i.d. standard uniform random variables. The transformed variable representing the jump amplitudes reduces to the standard uniform for n=1 and takes values in [0,1] for all values of n. In particular, $X^{(1)}$ is a compound Poisson-uniform process, which result has been discovered as a special case of fractionally integrated Poisson processes in [Orsingher and Polito, 2013] [52].

The first LT (4.1.1) cannot be evaluated explicitly 5 except for n=1, in which case it is $\phi_{\tilde{X}_1^{(1)}}(u)=\exp(\lambda((1-e^{-u})/u-1))$. Nonetheless, the first integral in (4.1.1) is very amenable to numerical computations using a standard Gauss–Kronrod quadrature rule because the integrand is an increasing function (of $s\in[0,1)$) with values in $[e^{-u},1]$ for any $u\geq0$.

Likewise, under the second recipe, the following representation exists for $Y^{(n)}$:

$$Y_t^{(n)} \stackrel{\text{d.}}{=} \sum_{k=1}^{X_t} e^{-Q(n, 1 - U_k)}, \quad t \ge 0,$$
(4.1.4)

which is also a compound Poisson process. Similar to the type I, the jump amplitudes are all valued in [0, 1], and are standard uniformly distributed for n = 1.

⁵Apparently, this is caused by the lack of an explicit antiderivative of the function $e^{-s}s^s$, $s \in [0,1)$. Even so, one can always derive alternative series representations for the log-LT.

For the same reason as the first, the second LT in (4.1.1) can be efficiently carried out as a numerical integral thanks to the monotonicity and boundedness of the integrand, while an explicit expression has been given for integer regulation degrees. Only for two degree values can it be expressed in terms of more elementary functions. Of course, if n=1, we have the compound Poisson-uniform LT $\phi_{\tilde{X}_1^{(1)}}(u) = \exp(\lambda((1-e^{-u})/u-1)) = \phi_{\tilde{X}_1^{(1)}}(u)$. If n=2, one can consult [Bateman, 1954, Eq. 4.6.1 and Eq. 4.6.2] [10] to obtain

$$\phi_{\tilde{X}_1^{(2)}}(u) = \exp\left(\lambda \left(\frac{\log u + \Gamma(0, u) - \Gamma'(1)}{u} - 1\right)\right),\,$$

where $-\Gamma'(1) \approx 0.577216$ is known as the Euler–Mascheroni constant.

Due to simplicity, the third LT in (4.1.1) (under the third recipe) permits explicit evaluation for any real regulation degree, from which we have the representation

$$Z_t^{(n)} \stackrel{\text{d.}}{=} \frac{1}{\Gamma(n+1)} \sum_{k=1}^{X_t} (1 - U_k)^n \stackrel{\text{d.}}{=} \frac{1}{\Gamma(n+1)} \sum_{k=1}^{X_t} B_{k,(1/n,1)}, \quad t \ge 0, \tag{4.1.5}$$

showing that $Z^{(n)}$ is a compound Poisson process with $1/\Gamma(n+1)$ -scaled beta(1/n,1)-distributed jumps. Unlike the other two types, due to such scaling the support of the jump amplitudes of $Z^{(n)}$ shrinks with n, and converges to the origin in its lower limit.

According to (4.1.3), (4.1.4), and (4.1.5), we conclude that when X is a Poisson process, all three types of regulated clocks follow compound Poisson processes with bounded jumps. These representations provide easy ways for conducting simulations. Also, the two corresponding transformations under the first two recipes form inverse functions of each other, in line with the demonstration by Figure 1.

In financial applications, compound Poisson processes with finite jump amplitudes, coupled with an independent Brownian motion, form adequate jump–diffusion models for log-price dynamics when sudden movements in returns are believed not to be arbitrarily large in reality; see [Yan and Hanson, 2006] [69] and also [Baustian et al., 2017] [12]. These models are built from uniform distributions and are deemed to enlarge the tail heaviness of Gaussian distributions to an extent comparable to normally or double-exponentially distributed jumps (e.g., [Kou, 2002] [40]). Noted that $X^{(1)}$ is a compound Poisson-uniform process, they can be simply expressed in terms of

$$\xi_t^{(1),X/b} + \sigma W_t = \mu t + \sigma W_t + \sum_{k=1}^{X_t} \frac{U_k}{b}, \quad t \ge 0$$
(4.1.6)

for a rate (reciprocal scale) parameter b>0 and a Brownian dispersion parameter $\sigma>0$. Since the continuous part $(\mu t + \sigma W_t)$ is immune to regulation by the stability of the Gaussian distribution, clock regulation can still be understood on the entire jump–diffusion process $\xi_t^{(1),X/b}+\sigma W_t$. Viewing from the representations (4.1.3), (4.1.4), and (4.1.5), the effect of regulation is then to assign greater (probabilistic) weights to smaller price jumps, and the consequent jump amplitude distribution, which possesses a strictly decreasing density over a finite domain, is a "give-and-take" between the uniform and the exponential family.

To give an example, let us consider the scaled clock X/b_n , where b_n is for every n>0 a rate parameter (assuming $b_0=1$ for simplicity), and derive from it the regulated clocks $X^{(n)}$, $Y^{(n)}$, and $Z^{(n)}$ accordingly, whose constant mixtures are constructed following Subsection 3.1, with $\mu=0$ and $\kappa_1=\kappa_2=1$. Then the processes $\xi^{(n),X}$, $\xi^{(n),Y}$, and $\xi^{(n),Z}$ are centered symmetric compound

Poisson processes with intensity λ and positive and negative jumps equally distributed in magnitude. To fix the variance of $\xi^{(n),X}$ (at generic time) over n, it suffices to set $b_n = \sqrt{C_{2,n}}$, for $\xi^{(n),Y}$, $b_n = 3^{-n/2}$, and for $\xi^{(n),Z}$, $b_n = 1/(\sqrt{2n+1}\Gamma(n+1))$. Then, as n increases, the domain of jump amplitudes spreads out, albeit bounded, and the probability of smaller jumps also rises, as Figure 3 shows. Therefore, $\xi^{(n),X}$, $\xi^{(n),Y}$, and $\xi^{(n),Z}$ all constitute a rich class of desirable models, when return jumps are known to be bounded in size but unevenly distributed.

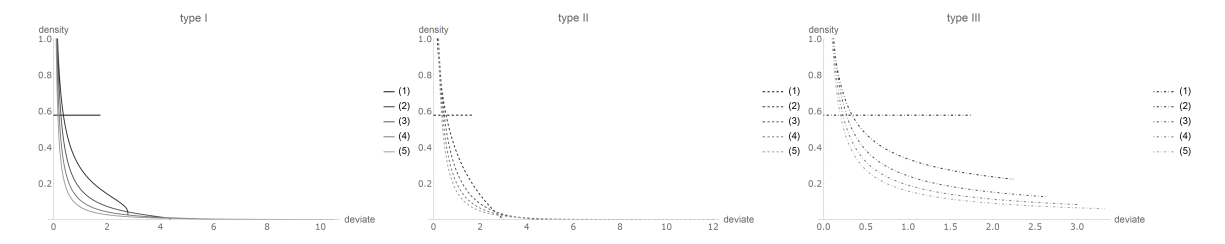


Figure 3: Distorted uniform distributions of (positive) jumps for fixed variance

Moreover, if X and X' are two independent Poisson processes with possibly different intensities, say $\lambda, \lambda' > 0$, the modified constant mixture $\xi^{X,X'}/b$ with parameters $\delta > 0$, $\mu = 0$, and $\kappa_1 = \kappa_2 = 1$ is seen to be a scaled Skellam process which has jumps of fixed amplitude (equal to 1/b). This type of discrete-valued processes have gained popularity in modeling tick-by-tick price changes with high-frequency data, as pioneered in [Barndorff-Nielsen et al., 2011] [9]. Recent developments have dealt with stochastic-volatility extensions for memory effects; see, e.g., [Kerss et al., 2014 [38], and [Gupta et al., 2020 [33], the latter also having studied associated running average processes beside discussing natural applications to scoring in ball sports. In connection with this, the process $\bar{X}^{(n)} - \bar{X}'^{(n)}$ $(n \in \mathbb{N}_{++})$, up to scaling by a positive number, defines exactly the ndegree running average of ξ^X (by linearity) and enables analysis of arbitrarily long-term behaviors of such phenomena (tick price changes versus scoring gaps). On the other hand, the scaled Lévy processes $\xi^{(n),X,X'}/b$, $\xi^{(n),Y,Y'}/b$, and $\xi^{(n),Z,Z'}/b$ of possibly fractional degrees n > 0, when applied for the same modeling purposes, allow for imprecision (e.g., ambiguity between change versus no change) in possible outcomes, by assigning positive probability to jumps of amplitudes strictly less than 1/b. In consequence, these possible outcomes are extended to real values to balance out false judgments, but still cannot fall out of their constructional range (tick sizes or score scales). In particular, the extent of imprecision is directly related to n – if $n \in (0,1)$, ambiguity in favor of no change stays minor. Obviously, in the limit as $n \setminus 0$ the original discrete-valued processes are restored.

4.2 Tempered stable subordinators

Tempered stable distributions are an infinitely divisible family that was initially introduced in [Koponen, 1995] [39] from a procedure incorporating the finite moments property of Gaussian processes into Lévy stable processes, where it bore the name "truncated Lévy flights." It is most commonly known in its one-sided form, characterized by up to three parameters a>0 (shape), b>0 (rate) and $c\in[0,1)$ (family), with which the corresponding Lévy processes are often called tempered stable subordinators and so are readily usable as stochastic clocks. We refer to [Schoutens,

⁶The superscript is expanded to include the process X' because here it is not an exact copy of X.

2003, Sect. 5.3.6] [59], [Rosiński, 2007] [56], and [Küchler and Tappe, 2013] [41] for a comprehensive treatment of these processes; see also [Grabchak, 2021] [31] for their discrete-valued analogy. The tempered stable family includes several commonly used subordinators as special cases, such as the gamma process (c = 0) and the inverse Gaussian process (c = 1/2). If X is a tempered stable subordinator with parametrization {a, b, c}, its LT (at t = 1) is given by

$$\phi_{X_1}(u) = \begin{cases} \exp(a\Gamma(-c)((u+b)^c - b^c)) & \text{if } c \in (0,1) \\ \left(\frac{u}{b} + 1\right)^{-a} & \text{if } c = 0, \end{cases} \quad u \in \mathbb{C} \setminus (-\infty, -b],$$

which is right-continuous at c=0. The Lévy density ℓ of X exists and equals $\ell(z)=ae^{-bz}/z^{c+1}$, z>0.

For n=1, the indistinguishable order-1 regulated clocks $X^{(1)}$, $Y^{(1)}$, and $Z^{(1)}$ have been studied in depth in [Xia, 2021] [68], by the name of "average-tempered stable subordinators." For all other values of n>0, in the presence of the gamma-related functions, for the type I it does not seem possible to further write the corresponding formulae in (2.1.5) and (2.2.3) explicitly, whereas both in the present form can be computed numerically with high efficiency thanks to the positivity and boundedness of the integrands.

In contrast, the formulae in (2.1.5) and (2.2.3) for the type-II clocks are reducible to some closed-form expressions provided $n \in \mathbb{N}_{++}$, by exploiting series representations of the integrands; further, due to the constructional simplicity of the type III, its corresponding formulae readily permit explicit evaluation, even for fractional degrees, which results are given in Proposition 2.

Proposition 2. If X is a tempered stable subordinator with with parametrization $\{a, b, c\}$, then for any n > 0,

$$\phi_{\bar{X}_{1}^{(n)}}(u) = \begin{cases} \exp\left(ab^{c}\Gamma(-c)\left(\frac{n+1}{n}F_{n}\left(1,\dots,1,-c;2,\dots,2;-\frac{u}{b}\right)-1\right)\right) & \text{if } c > 0 \\ e^{an}\left(\frac{u}{b}+1\right)^{-a(b/u+1)} \exp\left(\frac{ab}{u}\sum_{j=2}^{n}\operatorname{Li}_{j}\left(-\frac{u}{b}\right)\right) & \text{if } c = 0, \end{cases}$$

$$u \in \mathbb{C} \setminus (-\infty,-b], \ n \in \mathbb{N}_{++},$$

$$\phi_{\bar{X}_{t}^{(n)}|c>0}(u) = \begin{cases} \exp\left(atb^{c}\Gamma(-c)\left({}_{2}F_{1}\left(-c,\frac{1}{n};\frac{1}{n}+1;-\frac{u}{b\Gamma(n+1)}\right)-1\right)\right) & \text{if } c > 0 \\ \left(1+\frac{u}{b\Gamma(n+1)}\right)^{-at} \exp\left(\frac{atnu}{b\Gamma(n+2)} {}_{2}F_{1}\left(1,\frac{1}{n}+1;\frac{1}{n}+2;-\frac{u}{b\Gamma(n+1)}\right)\right) & \text{if } c = 0, \end{cases}$$

$$u \in \mathbb{C} \setminus (-\infty,-b\Gamma(n+1)], \ n > 0, \tag{4.2.1}$$

where $\operatorname{Li}_j(\cdot) = \sum_{k=1}^{\infty} (\cdot)^k k^{-j}$ the poly-logarithm, and where analytic continuation is understood in each slit region $(D_0(b))^{\complement} \setminus (-\infty, -b]$ and $(D_0(b\Gamma(n+1)))^{\complement} \setminus (-\infty, -b\Gamma(n+1)]$, n > 0, respectively, and

$$\tilde{\ell}^{(n)}(z) = ab^{c+1}G_{n,n+1}^{n+1,0} {1, \dots, 1 \atop 0, \dots, 0, -c-1} bz, \quad z > 0, \ n \in \mathbb{N}_{++},$$

$$\tilde{\ell}^{(n)}(z) = \frac{ab^{c}(b\Gamma(n+1)z)^{1/n}\Gamma(-c-1/n, b\Gamma(n+1)z)}{nz}, \quad z > 0, \ n > 0,$$
(4.2.2)

where $G_{\cdot,\cdot}^{\cdot,\cdot}(\cdots|\cdot)$ denotes the Meijer *G*-function (see the proof in Appendix A).

Note that if n=1, then with $_2F_1(1,-c;2;-u/b)=(b^{-c}(u+b)^{c+1}-b)/((c+1)u)$ and $\sum_{j=2}^1\equiv 0$ the elementary formulae follow:

$$\phi_{\tilde{X}_1^{(1)}|c>0}(u) = \exp\frac{a\Gamma(-c)((u+b)^{c+1} - b^c((c+1)u+b))}{(c+1)u}, \quad \phi_{\tilde{X}_1^{(1)}|c=0}(u) = e^a \left(\frac{u}{b} + 1\right)^{-a(b/u+1)},$$

as were initially obtained in [Xia, 2021, Thm. 1 and Corol. 2] [68]. For rational values of the family parameter $c \in (0,1)$, it is possible to rewrite (4.2.1) in terms of multiply nested sums of polylogarithms; see, e.g., [Kalmykov and Kniehl, 2009] [36]. However, it is our preference not to straggle into those representations which are extremely lengthy in general, as interest is more for computational efficiency. For example, the following elementary formula applies to n = 2 in the special case c = 1/2, corresponding to the inverse Gaussian process:

$$\phi_{\tilde{X}_{1}^{(2)}|c=\frac{1}{2}}(u) = \left(\frac{1}{2}\left(\sqrt{\frac{u}{b}+1}+1\right)\right)^{8a\sqrt{b^{3}\pi}/(3u)} \exp\left(2a\sqrt{b\pi}\left(\frac{4b}{9u}\left(4-\left(\frac{u}{b}+4\right)\sqrt{\frac{u}{b}+1}\right)+1\right)\right).$$

It can be easily verified using the antiderivative of $(\log v)\sqrt{uv+b}$ in $v \in (0,1)$; see [Gradshteyn and Ryzhik, 2007, Eq. 2.725] [32].

Also, we note that none of the Lévy densities given in (4.2.2) is integrable on \mathbb{R}_{++} , meaning that the processes $Y^{(n)}$'s all have essentially infinite jump activity, as discussed earlier; in particular, for the tempered stable subordinator $\mathfrak{B}(X^{(n)}) = \mathfrak{B}(Y^{(n)}) = \mathfrak{B}(Z^{(n)}) = \mathfrak{B}(X) = c \in [0,1)$. In the special case n=1, the first formula in (4.2.2) reduces to

$$\tilde{\ell}^{(1)}(z) = ab^{c+1}\Gamma(-c-1, bz), \quad z > 0,$$

corresponding to the Lévy density derived in [Xia, 2021, Corol. 1] [68], while for $n \ge 2$, the formula (4.2.2) stands and cannot be simplified to more elementary functions.⁷

Unlike the other two, the third recipe benefits by having no effect of increasing the computational complexity of the LT when operating on a tempered stable subordinator,⁸ and by this advantage the formulae (4.2.1) can be confidently applied to characteristic function-based optimization problems such as calibrating the parameters of a market model on strings of derivatives prices using numerical Fourier transforms.

Because the LTs $\phi_{\tilde{X}_t^{(n)}}$, $\phi_{\tilde{X}_t^{(n)}}$, and $\phi_{\tilde{X}_t^{(n)}}$ (fixing t>0) are all analytic in the complex plane except for a branch point on the negative real axis, the corresponding inverses (i.e., (a posteriori existent) density functions) can be found via a standard deformation argument employing a counterclockwise keyhole contour avoiding the cut extending to $-\infty$. Consequently, we obtain the following formulae:

$$\begin{split} f_{\bar{X}_{t}^{(n)}}(x) &:= \frac{\mathsf{P}\big\{\bar{X}_{t}^{(n)} \in \mathsf{d}x\big\}}{\mathsf{d}x} = \frac{1}{\pi} \int_{b}^{\infty} \mathsf{d}u \, \exp\big(\mathsf{Relog}\phi_{\bar{X}_{t}^{(n)}}(e^{\mathsf{i}\pi}u) - ux\big) \sin\big(-\mathsf{Imlog}\phi_{\bar{X}_{t}^{(n)}}(e^{\mathsf{i}\pi}u)\big), \\ f_{\bar{X}_{t}^{(n)}}(x) &:= \frac{\mathsf{P}\big\{\bar{X}_{t}^{(n)} \in \mathsf{d}x\big\}}{\mathsf{d}x} = \frac{1}{\pi} \int_{b}^{\infty} \mathsf{d}u \, \exp\big(\mathsf{Relog}\phi_{\bar{X}_{t}^{(n)}}(e^{\mathsf{i}\pi}u) - ux\big) \sin\big(-\mathsf{Imlog}\phi_{\bar{X}_{t}^{(n)}}(e^{\mathsf{i}\pi}u)\big), \end{split}$$

 $^{^{7}}$ The first formula (4.2.2) is not really useful beyond deciphering the functional form of the induced Lévy densities; more specifically, because the G-function is defined through complex line integration by most computer algebra systems, its implementation is understandably much less computationally efficient relative to its numerical counterpart (via (2.2.3) by the quadrature rule), which also accommodates fractional values of n.

⁸Numerical computations through the formulae (4.2.1) and (4.2.2) still intensify with the regulation degree $n \in \mathbb{N}_{++}$ which controls the dimensionality of the hypergeometric functions.

$$f_{\check{X}_{t}^{(n)}}(x) := \frac{\mathsf{P}\{\check{X}_{t}^{(n)} \in \mathsf{d}x\}}{\mathsf{d}x} = \frac{1}{\pi} \int_{b\Gamma(n+1)}^{\infty} \mathsf{d}u \, \exp\left(\mathsf{Re}\log\phi_{\check{X}_{t}^{(n)}}(e^{\mathsf{i}\pi}u) - ux\right) \sin\left(-\mathsf{Im}\log\phi_{\check{X}_{t}^{(n)}}(e^{\mathsf{i}\pi}u)\right) \tag{4.2.3}$$

for x, t > 0, where the real and imaginary parts are efficiently computable according to Theorem 1. In particular, for $n \in \mathbb{N}_{++}$ we have, after the substitution $u/b \mapsto 1/\gamma$

$$f_{\tilde{X}_{t}^{(n)}|c>0}(x) = \frac{be^{-atb^{c}\Gamma(-c)}}{\pi} \int_{0}^{1} \frac{\mathrm{d}y}{y^{2}} \exp\left(atb^{c}\Gamma(-c)\operatorname{Re}_{n+1}F_{n}\left(1,\dots,1,-c;2,\dots,2;\frac{1}{y}\right) - \frac{bx}{y}\right) \times \sin\left(-atb^{c}\Gamma(-c)\operatorname{Im}_{n+1}F_{n}\left(1,\dots,1,-c;2,\dots,2;\frac{1}{y}\right)\right), \quad x>0$$
(4.2.4)

and for any n > 0, with $u/(b\Gamma(n+1)) \mapsto 1/\gamma$,

$$f_{\check{X}_{t}^{(n)}|c>0}(x) = \frac{b\Gamma(n+1)e^{-atb^{c}\Gamma(-c)}}{\pi} \int_{0}^{1} \frac{\mathrm{d}y}{y^{2}} \exp\left(atb^{c}\Gamma(-c)\operatorname{Re}{}_{2}F_{1}\left(-c,\frac{1}{n};\frac{1}{n}+1;\frac{1}{y}\right) - \frac{b\Gamma(n+1)x}{y}\right) \\ \times \sin\left(-atb^{c}\Gamma(-c)\operatorname{Im}{}_{2}F_{1}\left(-c,\frac{1}{n};\frac{1}{n}+1;\frac{1}{y}\right)\right), \quad x>0. \tag{4.2.5}$$

Despite stability, implementation of (4.2.4) will require some effort for $n \ge 2$ since the hypergeometric functions need to be computed by analytic continuation of the definitional series which are only convergent within $D_0(1)$, while there is no such issue for (4.2.5) because of fixed dimensionality of the hypergeometric functions.

With its overall flexibility and explicitness, processes with marginal tempered stable distributions are of great applicability in operations research, especially in the fields of reliability engineering and mathematical finance; we mention [van Noortwijk, 2009] [65], [Wang and Xu, 2015] [66], and [Ye and Xie, 2015] [70] for résumés on related structural degradation models and [Boyarchenko and Levendorskii, 2000] [17] and [Carr et al., 2002] [18] for derivatives pricing theory. For Gaussian mixtures, the path regularity is directly captured by the family parameter $c \in [0,1)$. Recalling that $\mathfrak{B}(\Xi^X) = \mathfrak{B}(\Xi^{(n),X}) = \mathfrak{B}(\Xi^{(n),Y}) = \mathfrak{B}(\Xi^{(n),Z}) = 2c$, for any n > 0 (by Corollary 6), if $c \in [0,1/2)$, then the mixed processes $\Xi^{(n),X}$, $\Xi^{(n),Y}$, and $\Xi^{(n),Z}$ all have sample paths of finite variation, while the paths are of infinite variation for $c \in [1/2,1)$. In the special cases c = 0 and c = 1/2, Ξ^X becomes the variance gamma process and the normal inverse Gaussian process, respectively. With $\mathfrak{B}(X) = 0$ the sample paths of the variance gamma process are of finite variation while with $\mathfrak{B}(X) = 1$ those of the normal inverse Gaussian process have infinite variation. In such cases, the processes $\Xi^{(n),X}$, $\Xi^{(n),Y}$, and $\Xi^{(n),Z}$ derived from stochastic clock regulation are natural extensions of the foregoing models with arbitrarily large skewness and kurtosis, the mean and variance fixed and path regularity unchanged.

Subject to the addition parameters $\mu, \theta \in \mathbb{R}$, the density function of $\Xi_t^{(n),X}$ can be written either with (3.2.2) as the Fourier inverse

$$f_{\Xi_t^{(n),X}}(x) := \frac{\mathsf{P}\{\Xi_t^{(n),X} \in \mathrm{d}x\}}{\mathrm{d}x} = \frac{1}{\pi} \int_0^\infty \mathsf{Re}(e^{-\mathrm{i}ux} \phi_{\Xi_t^{(n),X}}(-\mathrm{i}u)) \mathrm{d}u$$

⁹From a computational viewpoint, the formulae in (4.2.3) are stabler than performing a numerical inverse Fourier transform and allow the density functions to evaluated (or plotted) on a fine grid.

 $^{^{10}}$ In [Carr et al., 2002] [18], two-sided tempered stable processes were studied under the name "CGMY," which include the variance gamma process as a special case. However, for $c \neq 0$ such processes cannot be interpreted as Gaussian mixtures of tempered stable subordinators.

$$= \frac{1}{\pi} \int_0^\infty \operatorname{Re}\left(e^{\mathrm{i}(\mu t - x)u} \phi_{\bar{X}_t^{(n)}}\left(-\mathrm{i}\theta u + \frac{u^2}{2}\right)\right) \mathrm{d}u, \quad x \in \mathbb{R}, \ t > 0$$
 (4.2.6)

or, after applying the Bayes theorem to (4.2.3), as the marginalization

$$\begin{split} f_{\Xi_{t}^{(n),X}}(x) &= \int_{0}^{\infty} \frac{\mathrm{d}w}{\sqrt{2\pi w}} e^{-(x-\theta w)^{2}/(2w)} f_{\bar{X}_{t}^{(n)}}(w) \\ &= \frac{1}{\pi} \int_{b}^{\infty} \frac{\mathrm{d}u}{\sqrt{2u+\theta^{2}}} \exp\left(\text{Re} \log \phi_{\bar{X}_{t}^{(n)}}(e^{\mathrm{i}\pi}u) + \theta(x-\mu t) - |x-\mu t| \sqrt{2u+\theta^{2}} \right) \\ &\quad \times \sin\left(-\operatorname{Im} \log \phi_{\bar{X}_{t}^{(n)}}(e^{\mathrm{i}\pi}u) \right), \end{split} \tag{4.2.7}$$

where the use of Fubini's theorem in the second equality is under the condition that c < 1/2, similar results hold for the densities $f_{\Xi^{(n),Y}}$ and $f_{\Xi^{(n),Z}}$ in terms of $\phi_{\tilde{X}^{(n)}}$ and $\phi_{\tilde{X}^{(n)}}$, respectively.

It is straightforward to keep the mean and variance of the Gaussian mixture $\Xi^{(n),Y}$ invariant to n with the parametrization $\{a,b,\mu,\theta\}$. One can for example adjust the location and Brownian drift parameters μ and θ according to the rules $\mu_n + \theta_n \mathsf{E} X_1/2^n = [\text{target mean}]$ and $\mathsf{E} X_1/2^n + \theta_n^2(\mathsf{Var} X_1)/3^n = [\text{target variance}];^{12}$ to maintain the moderate enlargement effects in (2.3.5), one can as well adjust the location and (tempered stable) rate parameters μ and b by the rules $\mu_n + \theta \mathsf{E} X_1/(2^n b_n) = [\text{target mean}]$ and $\mathsf{E} X_1/(2^n b_n) + \theta^2(\mathsf{Var} X_1)/(3^n b_n^2) = [\text{target variance}]$, where X_1 has unit scale; alternatively, disregarding the additional parameters μ and θ one can change the shape and rate parameters a and b of the unregulated clock a, as discussed in Subsection 3.2. Along these lines one can come up with many hybrid methods for fixing the mean and variance, e.g., by changing a, a and powers of a simultaneously. Similar arguments go for a

5 Optimal degrees of regulation

It is time to consider the problem of finding an optimal degree n of regulation with available data. Optimization may be accomplished by many different rules, depending on various aspects of the resultant distributions and data types. Instead of a comprehensive analysis, the aim of this section is to discuss two popular and comfortable methods that can justify values significantly deviating from zero (unregulated case) with due contrast control. The methods by themselves accommodate both the constant mixture ξ^X and the Gaussian mixture Ξ^X .

5.1 Moment-based estimation

In financial modeling, it is a standard assumption that a probability distribution of asset returns can be defined by the knowledge of their first several (usually four) moments; see, e.g., [Ané and Geman, 2000] [5]. This suggests that one can use the first sample moments – in particular the sample mean, variance, skewness, and excess kurtosis – to retrieve certain model parameters, and underlies our moment-based estimation procedure, which goes as follows.

¹¹It can be shown that the polarity of $\operatorname{Relog} \phi_{X_t}(e^{\mathrm{i}\pi}u)$ with X being a tempered stable subordinator exactly equals that of 2c-1, which feature is also unaffected by regulation (n).

¹²Since we know from Subsection 3.2 that the value of θ directly controls the skewness, this approach can very quickly result in abnormally large asymmetry as *n* increases.

 $^{^{13}}$ In contrast to the first, this one tends to give milder-than-moderate enlargement effects and so can fit in with a wide range of values of n, hence also more manageable; see Appendix B for details.

We start by fixing a truncated and discretized domain $\mathfrak{N} \subsetneq \mathbb{R}_+$ of degrees of regulation, and conduct moment-based estimation of the model parameters for each $n \in \mathfrak{N}$, with n = 0 corresponding to the unregulated case. Recall that regulation leads to simple cumulant reduction relations (Corollary 2), with regulation type-specific coefficients

$$\rho(m,n) := \begin{cases} C_{m,n} & \text{type I} \\ \frac{1}{(m+1)^n} & \text{type II} & m \in \mathbb{N}_{++}, \ n \ge 0, \\ \frac{1}{(mn+1)\Gamma^m(n+1)} & \text{type III}, \end{cases}$$
(5.1.1)

so it is most convenient to construct corresponding moment conditions from the model cumulants; for similar estimation procedures in the literature we refer to [Beckers, 1981] [13] and [Bandi and Nguyen, 2003] [6]. After experimenting with every member in \mathfrak{N} , the optimal value of n is identified (a posteriori) based on the maximal profile likelihood as a criterion for model selection. The reason behind choosing moment-based estimation over maximum likelihood estimation is twofold: It is much more computationally efficient because the density function of Lévy models are generally difficult to obtain in closed form (e.g., see [Schoutens, 2003, Chap. 4] [59]), with or without clock regulation; it is also more robust by making fewer assumptions for the underlying data-generating mechanism as only a finite number of moments are utilized.

Suppose that we have obtained an i.i.d. sample of some log-returns $\{\check{x}_k\}_{k=1}^N$, with $N\gg 1$ being the sample size, at a uniform frequency $\Delta>0$ in fractions of a year; from now on we shall write as [M], [V], [SK], and [EK] the sample mean, variance, skewness, and excess kurtosis, respectively, and $K_{\Delta}^{(n)}(m)$, for $m\in\{1,2,3,4\}$, the mixed model cumulants with regulation degrees $n\geq 0$. Then, the four moment conditions can be written

$$K_{\Delta}^{(n)}(1) = [M], \quad K_{\Delta}^{(n)}(2) = [V], \quad K_{\Delta}^{(n)}(3) = [SK][V]^{3/2}, \quad \frac{K_{\Delta}^{(n)}(3)}{K_{\Delta}^{(n)}(4)} = \frac{[SK]}{[EK][V]^{1/2}}.$$
 (5.1.2)

First, we take X to be a Poisson process and its constant mixture ξ^X plus an independent Brownian motion, as discussed in Subsection 4.1. From (4.1.3), (4.1.4), and (4.1.5) we know that in this case the model is of jump–diffusion type with bounded (distorted uniform) jumps. For convenience, we shall focus on downside jumps, in view of excessive tail risk, by imposing the auxiliary parameter values $\kappa_1 = 0$ and $\kappa_2 = 1$ in (3.1.1). Note that the mixed model with clock regulation has a total of four parameters to be estimated, including an infinite-divisibility parameter $\lambda_n > 0$, a rate parameter $b_n > 0$, a location parameter $\mu \in \mathbb{R}$, and a Brownian dispersion parameter $\sigma_n > 0$, all of which are subscripted by the corresponding degree of regulation, $n \ge 0$.

Proposition 3. Given any regulation degree $n \ge 0$, under the Poisson-based jump-diffusion model (see (4.1.6)) with $\kappa_1 = 0$ and $\kappa_2 = 1$ and parametrization $\{\lambda_n, b_n, \mu_n, \sigma_n\}$, the moment-based estimators are uniquely determined as

$$\hat{b}_n = \frac{|[SK]|}{[EK][V]^{1/2}} \frac{\rho(4,n)}{\rho(3,n)}, \quad \hat{\lambda}_n = \frac{|[SK]|[V]^{3/2} \hat{b}_n^3}{\Delta \rho(3,n)}, \quad \hat{\sigma}_n = \frac{[V]}{\Delta} - \rho(2,n) \frac{\hat{\lambda}_n}{\hat{b}_n^2}, \quad \hat{\mu}_n = \frac{[M]}{\Delta} + \rho(1,n) \frac{\hat{\lambda}_n}{\hat{b}_n}, \quad (5.1.3)$$

where $\rho(m, n)$'s are specified in (5.1.1).

In terms of the above estimates, the profile likelihood function under the mixed model (with an n-degree regulated clock) can be directly computed using the Bernoulli approximation technique

in [Kou, 2002, Eq. (5)] [40] as

$$\begin{split} \hat{g}_{\Delta}(n) &= \prod_{k=1}^{N} \Big(\Delta \int_{\mathbb{R}} \frac{\hat{b}_{n}}{\sqrt{2\pi\hat{\sigma}_{n}^{2}}} \exp\Big(-\frac{(\check{x}_{k} - z - \hat{\mu}_{n}\Delta)^{2}}{2\hat{\sigma}_{n}^{2}\Delta} \Big) \ell_{n}(-\hat{b}_{n}z) \mathrm{d}z \\ &+ (1 - \hat{\lambda}_{n}\Delta) \frac{1}{\sqrt{2\pi\hat{\sigma}_{n}^{2}}} \exp\Big(-\frac{(\check{x}_{k} - \hat{\mu}_{n}\Delta)^{2}}{2\hat{\sigma}_{n}^{2}\Delta} \Big) \Big), \end{split}$$

provided that Δ is small – e.g., as in the case of daily data, where the Lévy density ℓ_n represents any one of $\bar{\ell}_n$, $\tilde{\ell}_n$, and $\check{\ell}_n$ (with scaling factor $\hat{\lambda}_n$) in Proposition 1 according to the type of regulation. Whichever model yields the largest value of $\hat{g}_{\Lambda}(n)$ is taken as the best.

Second, we let X be a tempered stable subordinator and construct its Gaussian mixture Ξ^X . The family parameter $c \in [0,1)$ is fixed a priori for its special connection to local path regularity, which leaves us with also four parameters to be estimated – (with regulation degree subscripts) the infinite-divisibility parameter $a_n > 0$, rate parameter $b_n > 0$, location parameter $\mu \in \mathbb{R}$, and the Brownian drift parameter $\theta_n \in \mathbb{R}$. In this case, the moment-based estimators can be shown to be generally unique under the conditions in (5.1.2).

Proposition 4. Given any regulation degree $n \ge 0$, under the Gaussian-mixed tempered stable model with $c \in [0,1)$ and parametrization $\{a_n,b_n,\mu_n,\theta_n\}$, the moment-based estimators are given by the conditions

$$\hat{b}_{n} = \frac{2(2-c)\rho(3,n)\hat{\theta}_{n}^{2}}{\rho(2,n)P(|\hat{\theta}_{n}|)}, \quad \hat{a}_{n} = \frac{[V]\hat{b}_{n}^{1-c}}{\Delta\Gamma(1-c)(\rho(1,n)+(1-c)\rho(2,n)\hat{\theta}_{n}^{2}/\hat{b}_{n})},$$

$$\hat{\mu}_{n} = \frac{[M]}{\Delta} - \frac{\rho(1,n)\hat{\theta}_{n}[V]}{\Delta(\rho(1,n)+(1-c)\rho(2,n)\hat{\theta}_{n}^{2}/\hat{b}_{n})},$$
(5.1.4)

where $\hat{\theta}_n = \text{sgn}([SK])|\hat{\theta}_n|$ and $|\hat{\theta}_n|$ solves the rational equation

$$\frac{(3-c)\rho(2,n)\rho(4,n)}{4(2-c)\rho(3,n)^2}P^2(|\theta_n|) + \left(3 - \frac{[EK]|\theta_n|}{2|[SK]|}\right)P(|\theta_n|) + 3\left(1 - \frac{[EK]|\theta_n|}{|[SK]|}\right) = 0, \tag{5.1.5}$$

with

$$\begin{split} P(|\theta_n|) &= (|[SK]||\theta_n| - 3) + D^{1/2}(|\theta_n|), \\ D(|\theta_n|) &= (|[SK]||\theta_n| - 3)^2 + \frac{4(2-c)\rho(1,n)\rho(3,n)}{(1-c)\rho(2,n)^2} |[SK]||\theta_n|. \end{split}$$

With these estimates, the corresponding profile likelihood function is then simply $\hat{g}_{\Delta}(n) = \prod_{k=1}^{N} f_{\Xi_{\Delta}^{(n),\#}}(\check{x}_{k})$ (see (4.2.6) and (4.2.7)), where # is a placeholder for X, Y, or Z depending on the regulation type. Again, the best model is taken to be the one with the largest value of $\hat{g}_{\Delta}(n)$.

5.2 Model calibration on option prices

Alternatively, instead of estimating parameters from sample moments, one can recover them by model calibration on option price data. With the assumption of no-arbitrage, such an exercise will require that the LT be evaluated under some risk-neutral probability measure Q (other than P)

under which the asset price is discounted at some (supposedly) constant risk-free rate $r \ge 0$. Allowing for calibration efficiency, here we concentrate on the type-II and type-III regulated clocks which permit some explicit formulae when acting on Gaussian mixtures of tempered stable subordinators (recall Subsection 4.2). By way of the "mean-correcting measure" outlined in [Schoutens, 2003, Sect. 6.2.2] [59], we can then directly assume that the LT of the log asset price at time t > 0 under the measure Q is given by

$$\varphi_t(u;n) = \left(\frac{S_0 e^{rt}}{\phi_{\Xi_t^{(n),Y}}(-1)}\right)^{-u} \phi_{\Xi_t^{(n),Y}}(u) \quad \text{or} \quad \varphi_t(u;n) = \left(\frac{S_0 e^{rt}}{\phi_{\Xi_t^{(n),Z}}(-1)}\right)^{-u} \phi_{\Xi_t^{(n),Z}}(u), \quad n \in \mathfrak{N},$$

provided that the denominator in the power is finite, where $r \ge 0$ is the constant risk-free rate in the associated money market and \mathfrak{N} is the same select domain of the regulation degree n for experiments.

Then, the no-arbitrage price of a European-style call option written on S at time t=0 with strike price K and maturity T>0 fixed is given by

$$\Pi_0^{\text{call}}(n) = S_0 e^{-qT} Q_1(n) - K e^{-rT} Q_2(n), \tag{5.2.1}$$

where q > 0 is the (constant) dividend yield and

$$Q_{1}(n) = \frac{1}{2} + \frac{1}{\pi} \int_{0}^{\infty} \operatorname{Re} \frac{K^{-iu} \varphi_{T}(-iu - 1; n)}{iu \varphi_{T}(-1; n)} du, \quad Q_{2}(n) = \frac{1}{2} + \frac{1}{\pi} \int_{0}^{\infty} \operatorname{Re} \frac{K^{-iu} \varphi_{T}(-iu; n)}{iu} du$$

are associated risk-neutralized in-the-money probabilities.

Suppose that we have obtained contemporaneous market quotes of M call options on S for various strike prices and maturities, denoted as \check{H}^{call} . Focusing on the Gaussian mixed model Ξ^X where X is the tempered stable subordinator with a fixed family parameter $c \in [0,1)$, then after mean correction there will be only three parameters, a_n , b_n , and θ_n (with degree subscripts as before), whose (locally) optimal values can be found by solving the following minimization problem:

$$\{\hat{a}_{n}, \hat{b}_{n}, \hat{\theta}_{n}\} = \underset{a>0, b>0, \theta \in \mathbb{R}}{\operatorname{arg\,min}} \frac{1}{M} \sum_{K,T} \frac{|\check{\Pi}_{0}^{\operatorname{call}} - \Pi_{0}^{\operatorname{call}}(n)|}{\check{\Pi}_{0}^{\operatorname{call}}},$$
(5.2.2)

where the objective function is the mean absolute percentage error (MAPE) measuring average pricing errors and the summation runs over all available strikes and maturities. The best model is then characterized by imposing the criterion $\min_{n \in \mathfrak{N}}$ on the right side of (5.2.2). A similar exercise using put options is immediate by applying a standard parity argument to (5.2.1). Nevertheless, compared with moment-based estimation, calibration is expected to be less robust because it generally constitutes a highly non-convex optimization problem which must be solved numerically.

6 Empirical modeling

In this section we demonstrate the effect of clock regulation on real financial returns. We focus on the equity market and the cryptocurrency market; in particular, we have collected S&P500 index and Bitcoin price data on the daily basis over the 2020 calendar year (data source: *Yahoo Finance*) and have computed corresponding log-returns. The two data sets hence have sample sizes (N) of 252 and 366, respectively, with $\Delta = 1/252, 1/366$.

In accordance with the moment-based estimation procedures discussed in Subsection 5.1, our empirical study will feature two exercises, one using the constant mixture of a Poisson process augmented by an independent Brownian motion and the other using the Gaussian mixture of a tempered stable subordinator, respectively. We highlight that the first exercise is interesting for modeling (presumably) bounded jumps in asset returns ([Yan and Hanson, 2006] [69] and [Baustian et al., 2017] [12]) and aims to compare the distorted jump distributions with commonly used uniform distributions; the second, on the other hand, is especially significant for possible improvement of tempered stable processes ([Rosiński, 2007] [56] and [Küchler and Tappe, 2013] [41]) in terms of flexibility, by investigating how the degree n of regulation affects the model fit subject to moment matching for different choices of the family parameter c.

First, we report the four sample statistics of the collected return data in Table 1. Relative to the S&P500, Bitcoin returns have clearly exhibited a much larger (absolute) skewness and excess kurtosis, speaking to high asymmetrical and tail risk.

Table 1: Descriptive statistics of daily returns (~six significant digits)

Data set	mean	variance	skewness	excess kurtosis	
S&P500	0.000564705	0.00047912	-0.861012	8.46843	
Bitcoin	0.00384156	0.00160601	-4.07498	50.8679	

In both exercises, the choice of the degree domain is $\mathfrak{N} \subsetneq [0,10]$ with fixed modulus $|\mathfrak{N}| = 11$ to ease comparison. In the first exercise, the exponential jump–diffusion model ([Kou, 2002] [40]) is also included as a contrast model because the distorted uniform distributions due to regulation have exponential shapes. In the second exercise, we experiment with four values of c: 0 (variance gamma), 0.25, 0.5 (normal inverse Gaussian), and 0.75. Estimation results are presented in ten (sub)tables – Table 2(a), Table 2(b), Table 3(a), Table 3(b), Table 3(c), Table 3(d), Table 4(a), Table 4(b), Table 4(c), and Table 4(d), and are comprised of parameter estimates and the profile log-likelihood (PLL), $\log \hat{g}_{\Delta}(n)$, for every $n \in \mathfrak{N}$. In each model setting (including each chosen value of c), the model with the highest PLL value for a certain regulation type is marked " \star " and that with the highest PLL value taking into account all three types is marked " \star ". To enhance visual impact, changes in the PLL are plotted separately in Figure 4, Figure 6(a), and Figure 6(b).

Furthermore, we provide Figure 5, Figure 7(a), and Figure 7(b) to compare the estimated density functions of the best fit model (namely the one with the highest PLL value across all three types) and the original model (n = 0) against the empirical kernel density function which is estimated using the Gaussian kernel, i.e.,

$$\check{f}_{\Delta}(x) = \frac{1}{N\mathfrak{b}} \sum_{k=1}^{N} \frac{1}{\sqrt{2\pi}} e^{-(x-\check{x}_k)^2/(2\mathfrak{b}^2)}, \quad x \in \mathbb{R};$$

the optimal bandwidth b is determined by the Silverman rule of thumb:

$$\mathfrak{b} = \frac{0.9}{N^{1/5}} \min\left([V]^{1/2}, \frac{\mathrm{IQR}(\check{x})}{1.349} \right),$$

where IQR is the interquartile range (the difference between the third and the first quartiles).

Table 2(a): Jump diffusion estimation results on S&P500 daily returns (~six significant digits)

		î	î	^	^ :	DII		
	n	$\hat{\lambda}_n$	\hat{b}_n	$\hat{\mu}_n$	$\hat{\sigma}_n$	PLL		
	0	0.228049	4.64498	0.191402	0.331917	605.28		
	1	0.467045	3.71599	0.205148	0.330853	620.36		
	2	1.03524	3.37102	0.219081	0.330044	621.566		
	3	2.27627	3.11901	0.233531	0.329334	622.22		
	4	4.98085	2.91283	0.249179	0.328666	622.669		
type I	5	10.8658	2.73578	0.266423	0.328018	623.007		
••	6	23.6553	2.5796	0.285589	0.327377	623.276		
	7	51.4231	2.43945	0.306992	0.326739	623.496		
	8	111.664	2.31218	0.330954	0.326099	623.68		
	9	242.275	2.19558	0.357827	0.325455	623.837		
	10	525.314	2.08804	0.387992	0.324803	623.972*		
	n	$\hat{\lambda}_n$	\hat{b}_n	$\hat{\mu}_n$	$\hat{\sigma}_n$	PLL		
	0	0.228049	4.64498	0.191402	0.331917	605.28		
	1	0.467045	3.71599	0.205148	0.330853	620.36		
	2	0.956508	2.97279	0.222744	0.329716	621.973		
	3	1.95893	2.37823	0.245267	0.328497	622.917		
	4	4.01189	1.90259	0.274096	0.327193	623.557		
type II	5	8.21634	1.52207	0.310998	0.325796	624.018		
type II	6	16.8271	1.21765	0.358232	0.3243	624.359		
	7	34.4618	0.974124	0.418691	0.322695	624.612		
	8	70.5779	0.779299	0.496079	0.320976	624.798		
	9	144.543	0.623439	0.595135	0.319131	624.935		
	10	296.025	0.498751	0.721927	0.317151	625.046★		
	n	$\hat{\lambda}_n$	\hat{b}_n	$\hat{\mu}_n$	$\hat{\sigma}_n$	PLL		
	0	0.228049	4.64498	0.191402	0.331917	605.28		
	1	0.467045	3.71599	0.205148	0.330853	620.36		
	2	0.751093	1.80638	0.211606	0.330498	620.954		
	3	1.038	0.595511	0.214933	0.330338	621.161		
	4	1.32573	0.148002	0.216952	0.330247	621.267		
type III	5	1.6138	0.029492	0.218306	0.330189	621.33		
type III	6	1.90206	0.00490304	0.219277	0.330148	621.373		
	7	2.19041	0.000699163	0.220007	0.330118	621.404		
	8	2.47883	0.000087275	0.220576	0.330095	621.427		
	9	2.7673	9.68674×10^{-6}	0.221031	0.330077	621.445		
	10	3.05579	9.6783×10^{-7}	0.221404	0.330062	621.459 *		
exponential	-	2.43253	18.5799	0.273228	0.326566	624.048		

PLL: profile log-likelihood

Table 2(b): Jump diffusion estimation results on Bitcoin daily returns (~six significant digits)

	Ι		·					
	n	$\hat{\lambda}_n$	\hat{b}_n	$\hat{\mu}_n$	$\hat{\sigma}_n$	PLL		
	0	0.766746	1.99897	1.78958	0.62922	641.506		
	1	1.5703	1.59918	1.89698	0.618971	736.065		
	2	3.48068	1.45072	2.00583	0.611076	736.11		
	3	7.65327	1.34227	2.11873	0.604087	736.174		
	4	16.7466	1.25354	2.24098	0.597444	736.2★		
type I	5	36.533	1.17735	2.3757	0.590935	736.171		
	6	79.5338	1.11014	2.52544	0.584454	736.08		
	7	172.894	1.04982	2.69265	0.577936	735.924		
	8	375.437	0.995048	2.87986	0.571337	735.702		
	9	814.575	0.944869	3.08981	0.564624	735.414		
	10	1766.21	0.89859	3.32547	0.557771	735.063		
	n	$\hat{\lambda}_n$	\hat{b}_n	$\hat{\mu}_n$	$\hat{\sigma}_n$	PLL		
	0	0.766746	1.99897	1.78958	0.62922	641.506		
	1	1.5703	1.59918	1.89698	0.618971	736.065		
	2	3.21597	1.27934	2.03445	0.607849	736.076		
	3	6.5863	1.02347	2.21041	0.595756	736.101*		
	4	13.4887	0.81878	2.43565	0.582581	735.963		
type II	5	27.6249	0.655024	2.72395	0.568191	735.511		
type II	6	56.5759	0.524019	3.09297	0.552428	734.623		
	7	115.867	0.419215	3.56532	0.535103	733.21		
	8	237.297	0.335372	4.16992	0.515982	731.201		
	9	485.983	0.268298	4.94382	0.494772	728.473		
	10	995.294	0.214638	5.9344	0.471097	724.378		
	n	$\hat{\lambda}_n$	\hat{b}_n	$\hat{\mu}_n$	$\hat{\sigma}_n$	PLL		
	0	0.766746	1.99897	1.78958	0.62922	641.506		
	1	1.5703	1.59918	1.89698	0.618971	736.065		
	2	2.52532	0.777379	1.94743	0.615517	736.092		
	3	3.48997	0.256279	1.97342	0.613954	736.116		
	4	4.45737	0.0636928	1.9892	0.613067	736.131		
type III	5	5.42592	0.0126919	1.99977	0.612496	736.141		
type III	6	6.39508	0.00211003	2.00736	0.612097	736.148		
	7	7.36459	0.000300886	2.01306	0.611803	736.153		
	8	8.33432	0.0000375589	2.01751	0.611578	736.157		
	9	9.30419	4.1687×10^{-6}	2.02107	0.611399	736.16		
	10	10.2742	4.16507×10^{-7}	2.02398	0.611254	736.162*		
exponential	-	8.17863	7.9959	2.42886	0.576157	735.574		

PLL: profile log-likelihood

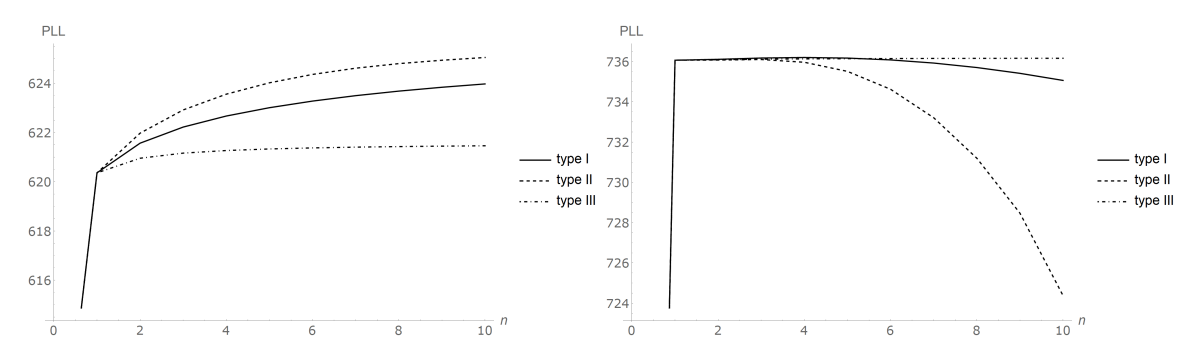


Figure 4: Jump diffusion log-likelihood with regulation degrees for S&P500 (left) and Bitcoin (right) daily returns

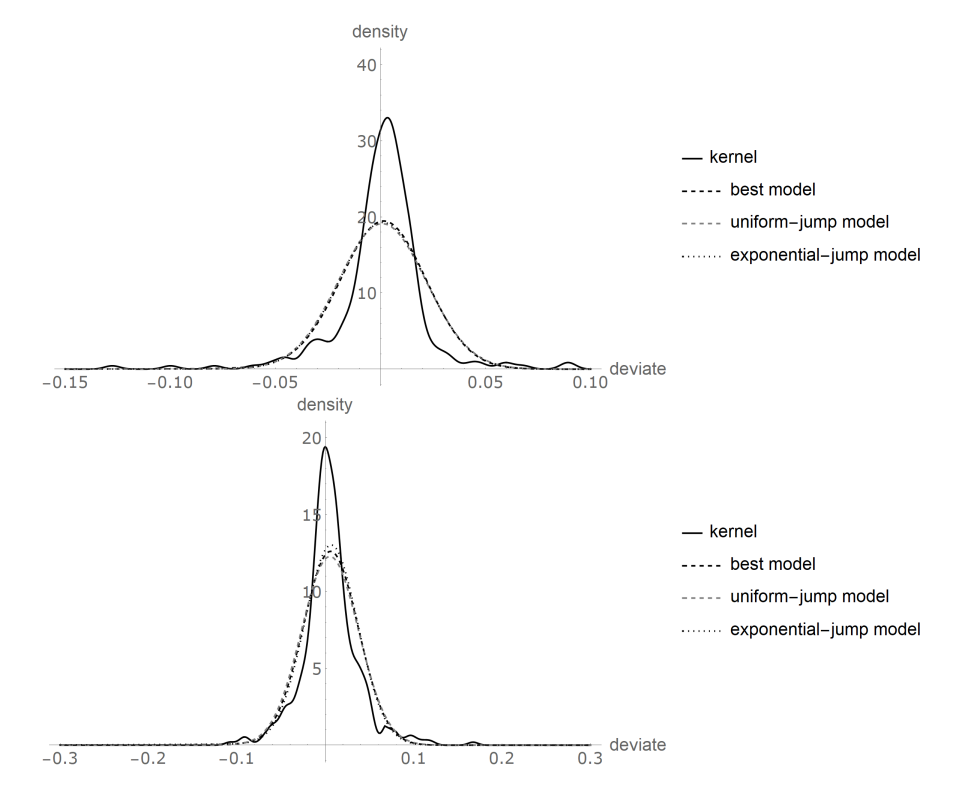


Figure 5: Jump diffusion estimated densities with regulation degrees for S&P500 (top) and Bitcoin (bottom) daily returns

Table 3(a): Tempered stable estimation results on S&P500 daily returns (~six significant digits)

	c = 0 (VG)									
	n	\hat{a}_n	\hat{b}_n	$\hat{\mu}_n$	$\hat{ heta}_n$	PLL				
	0	94.8367	811.158	0.744442	-5.1502	654.012				
	1	128.456	549.545	0.752422	-5.22027	662.425				
	2	203.096	434.589	0.760763	-5.29356	666.79				
	3	334.145	357.634	0.7691	-5.36685	668.065*				
	4	561.015	300.338	0.777794	-5.44332	667.986				
type I	5	954.266	255.534	0.787051	-5.52481	667.252				
typer	6	1638.64	219.491	0.797029	-5.6127	666.333				
	7	2835.01	189.959	0.807875	-5.70831	665.136				
	8	4935.86	165.446	0.81974	-5.81298	662.129				
	9	8641.45	144.906	0.832792	-5.92824	662.009				
	10	15206.5	127.574	0.847223	-6.05579	660.34				
	n	\hat{a}_n	\hat{b}_n	$\hat{\mu}_n$	$\hat{ heta}_n$	PLL				
	0	94.8367	811.158	0.744442	-5.1502	654.012				
	1	128.456	549.545	0.752422	-5.22027	662.425				
	2	174.38	373.157	0.761651	-5.30136	666.218				
	3	237.339	254.059	0.772375	-5.39565	667.676*				
	4	324.016	173.515	0.784904	-5.50592	667.625				
type II	5	443.949	118.945	0.799644	-5.63577	666.73				
- 7 F	6	610.907	81.8998	0.817127	-5.78997	665.336				
	7	845.057	56.6956	0.838074	-5.97499	663.626				
	8	1176.48	39.5076	0.863484	-6.19982	661.708				
	9	1651.07	27.7586	0.894794	-6.47743	659.645				
	10	2340.97	19.7109	0.93414	-6.82722	657.469				
	n	\hat{a}_n	\hat{b}_n	$\hat{\mu}_n$	$\hat{\theta}_n$	PLL				
	0	94.8367	811.158	0.744442	-5.1502	654.012				
	1	128.456	549.545	0.752422	-5.22027	662.425				
	2	174.86	249.402	0.756665	-5.25754	665.585				
	3	223.022	79.5317	0.758921	-5.27736	666.776				
	4	271.766	19.384	0.760309	-5.28957	667.32				
type III	5	320.774	3.81341	0.761249	-5.29782	667.615				
71	6	369.923	0.628261	0.761926	-5.30377	667.795				
	7	419.157	0.0889868	0.762437	-5.30826	667.915				
	8	468.446	0.0110503	0.762836	-5.31177	667.999				
	9	517.773	0.0012214	0.763157	-5.31459	668.061				
	10	567.126	0.000121622	0.76342	-5.31691	668.108★				

VG: variance gamma | PLL: profile log-likelihood

Table 3(b): Tempered stable estimation results on S&P500 daily returns (~six significant digits)

			c = 0.25	5		
	n	\hat{a}_n	\hat{b}_n	$\hat{\mu}_n$	$\hat{ heta}_n$	PLL
	0	11.8708	621.521	0.755058	-5.24342	668.251
	1	17.7616	422.34	0.764691	-5.32808	668.672★
	2	29.8475	335.05	0.774806	-5.41703	668.277
	3	51.6775	276.597	0.784966	-5.50645	667.305
	4	90.8543	233.057	0.795618	-5.60026	666.07
type I	5	161.326	198.997	0.807023	-5.70079	664.739
type i	6	288.564	171.591	0.819393	-5.80991	661.032
	7	519.198	149.132	0.832928	-5.92943	652.583
	8	938.875	130.495	0.847844	-6.06127	660.391
	9	1705.49	114.887	0.864387	-6.20765	659.088
	10	3111.25	101.731	0.882844	-6.37118	657.695
	n	\hat{a}_n	\hat{b}_n	$\hat{\mu}_n$	$\hat{ heta}_n$	PLL
	0	11.8708	621.521	0.755058	-5.24342	668.251
	1	17.7616	422.34	0.764691	-5.32808	668.672★
	2	26.6293	287.789	0.775895	-5.42662	668.241
	3	40.0192	196.745	0.789001	-5.54199	667.224
	4	60.311	135.026	0.804439	-5.67803	665.812
type II	5	91.1977	93.0987	0.82278	-5.83985	664.09
71	6	138.465	64.553	0.844796	-6.03439	662.253
	7	211.286	45.0713	0.871567	-6.27138	660.317
	8	324.434	31.744	0.904647	-6.56486	657.45
	9	502.195	22.6087	0.946369	-6.93602	655.531
	10	785.628	16.3417	1.0004	-7.41838	655.78
	n	\hat{a}_n	\hat{b}_n	$\hat{\mu}_n$	$\hat{ heta}_n$	PLL
	0	11.8708	621.521	0.755058	-5.24342	668.251
	1	17.7616	422.34	0.764691	-5.32808	668.672★
	2	29.4917	191.979	0.769827	-5.37324	668.582
	3	50.086	61.2722	0.772562	-5.39729	668.423
	4	86.8967	14.9415	0.774248	-5.41212	668.29
type III	5	154.046	2.94048	0.775389	-5.42216	668.186
71	6	278.893	0.484571	0.776211	-5.42939	668.103
	7	515.191	0.0686477	0.776833	-5.43486	668.038
	8	970.033	0.00852589	0.777318	-5.43913	667.985
	9	1859.66	0.000942492	0.777708	-5.44256	667.941
	10	3626.32	0.0000938585	0.778028	-5.44538	667.904

PLL: profile log-likelihood

Table 3(c): Tempered stable estimation results on S&P500 daily returns (~six significant digits)

			c = 0.5	(NIG)		
	n	\hat{a}_n	\hat{b}_n	$\hat{\mu}_n$	$\hat{ heta}_n$	PLL
	0	1.3704	432.849	0.777245	-5.43847	667.041★
	0.5	1.72512	343.139	0.783233	-5.49118	666.37
	1	2.26522	296.003	0.790516	-5.5553	665.447
	1.5	3.01643	262.598	0.797581	-5.61754	664.544
	2	4.04629	236.4	0.804581	-5.67924	663.674
type I	2.5	5.45309	214.807	0.811644	-5.74153	662.832
type i	3	7.37333	196.483	0.818859	-5.80518	662.016
	3.5	9.99496	180.635	0.826291	-5.87079	661.22
	4	13.5762	166.743	0.833993	-5.93881	660.442
	4.5	18.472	154.447	0.842012	-6.00967	659.68
	5	25.17	143.48	0.850391	-6.08376	658.933
	n	\hat{a}_n	\hat{b}_n	$\hat{\mu}_n$	$\hat{ heta}_n$	PLL
	0	1.3704	432.849	0.777245	-5.43847	667.041★
	0.5	1.76152	357.786	0.783616	-5.49455	666.261
	1	2.26522	296.003	0.790516	-5.5553	665.447
	1.5	2.9143	245.126	0.797999	-5.62123	664.604
	2	3.75125	203.209	0.806132	-5.69292	663.738
type II	2.5	4.83121	168.655	0.814989	-5.77105	662.853
- J F	3	6.22584	140.155	0.824658	-5.85639	661.951
	3.5	8.02838	116.634	0.835242	-5.94987	661.036
	4	10.3604	97.2105	0.846859	-6.05256	660.108
	4.5	13.3806	81.1608	0.859651	-6.16575	659.17
	5	17.2969	67.8906	0.87379	-6.29097	658.222
	n	\hat{a}_n	\hat{b}_n	$\hat{\mu}_n$	$\hat{ heta}_n$	PLL
	0	1.3704	432.849	0.777245	-5.43847	667.041★
	0.5	1.68675	371.306	0.784277	-5.50037	666.26
	1	2.26522	296.003	0.790516	-5.5553	665.447
	1.5	3.173	210.414	0.7947	-5.59216	664.868
	2	4.58808	135.007	0.797632	-5.61799	664.453
type III	2.5	6.81669	79.3114	0.799788	-5.63699	664.144
-J F	3	10.3757	43.1666	0.801435	-5.65151	663.907
	3.5	16.1436	21.9721	0.802734	-5.66296	663.719
	4	25.6301	10.5381	0.803784	-5.67221	663.567
	4.5	41.459	4.7913	0.804649	-5.67984	663.442
	5	68.2414	2.07545	0.805375	-5.68624	663.337

NIG: normal inverse Gaussian | PLL: profile log-likelihood

Table 3(d): Tempered stable estimation results on S&P500 daily returns (~six significant digits)

			c = 0.	.75		
	n	\hat{a}_n	\hat{b}_n	$\hat{\mu}_n$	$\hat{ heta}_n$	PLL
	0	0.127463	248.604	0.852286	-6.10039	654.027★
	0.1	0.134541	233.914	0.853433	-6.11053	653.976
	0.2	0.142421	222.685	0.855778	-6.13128	653.863
	0.3	0.151034	213.54	0.858568	-6.15597	653.721
	0.4	0.160364	205.785	0.861531	-6.18219	653.566
type I	0.5	0.170423	199.021	0.864556	-6.20896	653.405
type i	0.6	0.181235	193.002	0.867597	-6.23588	653.242
	0.7	0.192836	187.563	0.870632	-6.26276	653.079
	0.8	0.205268	182.593	0.873656	-6.28954	652.917
	0.9	0.218579	178.007	0.876666	-6.3162	652.757
	1	0.232824	173.745	0.879663	-6.34276	652.599
	n	\hat{a}_n	\hat{b}_n	$\hat{\mu}_n$	$\hat{ heta}_n$	PLL
	0	0.127463	248.604	0.852286	-6.10039	654.027★
	0.1	0.135368	239.776	0.854794	-6.12257	653.885
	0.2	0.143766	231.278	0.857349	-6.14518	653.743
	0.3	0.152687	223.097	0.859953	-6.16822	653.601
	0.4	0.162164	215.22	0.862607	-6.19171	653.458
type II	0.5	0.172233	207.637	0.865313	-6.21566	653.316
· J P · · · ·	0.6	0.182929	200.335	0.868072	-6.24008	653.173
	0.7	0.194293	193.306	0.870884	-6.26499	653.03
	0.8	0.206367	186.537	0.873753	-6.29039	652.887
	0.9	0.219194	180.02	0.876679	-6.31631	652.743
	1	0.232824	173.745	0.879663	-6.34276	652.599
	n	\hat{a}_n	\hat{b}_n	$\hat{\mu}_n$	$\hat{ heta}_n$	PLL
	0	0.127463	248.604	0.852286	-6.10039	654.027★
	0.1	0.132234	240.172	0.853793	-6.11372	653.96
	0.2	0.13829	233.905	0.856772	-6.14007	653.818
	0.3	0.14551	228.168	0.86014	-6.16988	653.65
	0.4	0.153881	222.222	0.863506	-6.19967	653.475
type III	0.5	0.163442	215.729	0.86672	-6.22812	653.305
- J F	0.6	0.174271	208.561	0.869727	-6.25475	653.143
	0.7	0.186477	200.706	0.872516	-6.27944	652.991
	8.0	0.200194	192.219	0.875092	-6.30226	652.85
	0.9	0.21558	183.194	0.877469	-6.32332	652.72
	1	0.232824	173.745	0.879663	-6.34276	652.599

PLL: profile log-likelihood

Table 4(a): Tempered stable estimation results on Bitcoin daily returns (~six significant digits)

			c = 0 (VC	G)		
	n	\hat{a}_n	\hat{b}_n	$\hat{\mu}_n$	$\hat{ heta}_n$	PLL
	0	27.7898	56.0074	3.00165	-3.21585	455.411
	1	39.9891	40.7099	3.10861	-3.46658	524.494
	2	67.5402	34.7769	3.23098	-3.75877	601.924
	3	119.117	31.0558	3.36652	-4.08912	655.587
	4	215.901	28.5552	3.52426	-4.48257	691.131
type I	5	400.41	26.9375	3.71367	-4.96792	715.837
type i	6	759.406	26.0819	3.94698	-5.58529	729.963
	7	1474.97	25.9914	4.24121	-6.39498	737.741
	8	2941.94	26.7808	4.62072	-7.49154	741.75
	9	6047.17	28.7032	5.12027	-9.02652	742.155★
	10	12850.6	32.2046	5.78719	-11.2431	740.616
	n	\hat{a}_n	\hat{b}_n	$\hat{\mu}_n$	$\hat{ heta}_n$	PLL
	0	27.7898	56.0074	3.00165	-3.21585	455.411
	1	39.9891	40.7099	3.10861	-3.46658	524.494
	2	58.4843	30.162	3.24722	-3.79825	591.811
	3	87.4167	22.9374	3.43303	-4.25497	645.474
	4	134.707	18.1054	3.69371	-4.91968	691.284
type II	5	217.137	15.123	4.08334	-5.96699	717.942
- J F	6	375.668	13.859	4.72003	-7.82461	730.62
	7	730.375	14.9641	5.89275	-11.7664	730.654*
	8	1689.11	21.4225	8.28461	-22.3332	716.365
	9	4447.82	42.7097	12.7363	-55.7046	675.673
	10	11431.1	114.716	19.1751	-182.6	558.882
	n	\hat{a}_n	\hat{b}_n	$\hat{\mu}_n$	$\hat{ heta}_n$	PLL
	0	27.7898	56.0074	3.00165	-3.21585	455.411
	1	39.9891	40.7099	3.10861	-3.46658	524.494
	2	56.2539	19.1976	3.16875	-3.60939	573.498
	3	73.0303	6.24998	3.20178	-3.6884	598.04
	4	89.9752	1.543	3.22249	-3.73814	613.948
type III	5	106.996	0.306219	3.23666	-3.77226	623.336
oj po III	6	124.059	0.05077	3.24696	-3.79711	630.002
	7	141.146	0.00722557	3.25478	-3.816	635.146
	8	158.249	0.000900634	3.26092	-3.83085	639.394
	9	175.363	0.0000998491	3.26587	-3.84282	642.235
	10	192.485	9.9672×10^{-6}	3.26994	-3.85268	644.439*

VG: variance gamma | PLL: profile log-likelihood

Table 4(b): Tempered stable estimation results on Bitcoin daily returns (~six significant digits)

			c = 0.25			
	n	\hat{a}_n	\hat{b}_n	$\hat{\mu}_n$	$\hat{ heta}_n$	PLL
	0	7.17612	47.0281	3.1418	-3.54481	641.25
	1	11.3467	35.0184	3.28923	-3.8994	674.554
	2	20.2654	30.7629	3.46274	-4.32733	703.597
	3	37.443	28.3513	3.66136	-4.83148	722.383
	4	70.7801	27.0578	3.90086	-5.45996	734.063
type I	5	136.543	26.7025	4.19975	-6.27619	740.223
typer	6	268.857	27.3237	4.5831	-7.3758	743.733
	7	541.024	29.136	5.08604	-8.91013	744.02★
	8	1113.88	32.5598	5.756	-11.1203	741.869
	9	2344.96	38.2747	6.65067	-14.3797	737.46
	10	5028.11	47.2474	7.82714	-19.2312	730.984
	n	\hat{a}_n	\hat{b}_n	$\hat{\mu}_n$	$\hat{ heta}_n$	PLL
	0	7.17612	47.0281	3.1418	-3.54481	641.25
	1	11.3467	35.0184	3.28923	-3.8994	674.554
	2	18.2308	26.8011	3.48754	-4.39002	701.452
	3	29.9485	21.3312	3.76679	-5.10797	721.23
	4	50.8037	18.0118	4.18535	-6.24526	733.655
type II	5	90.4781	16.731	4.86847	-8.26702	737.997*
JI	6	173.503	18.2688	6.10689	-12.5041	734.271
	7	364.579	25.7088	8.51289	-23.2474	718.548
	8	795.808	47.4225	12.7543	-53.8354	682.923
	9	1616.39	110.052	18.8531	-153.237	606.713
	10	2565.25	544.578	26.6876	-928.402	320.315
	n	\hat{a}_n	\hat{b}_n	$\hat{\mu}_n$	$\hat{ heta}_n$	PLL
	0	7.17612	47.0281	3.1418	-3.54481	641.25
	1	11.3467	35.0184	3.28923	-3.8994	674.554
	2	19.4167	16.7381	3.37351	-4.10569	692.703
	3	33.5171	5.48975	3.42025	-4.2212	701.522
	4	58.7421	1.36161	3.44971	-4.29443	706.549
type III	5	104.855	0.271079	3.46994	-4.34489	709.757
71	6	190.782	0.0450476	3.48468	-4.38175	711.971
	7	353.758	0.00642237	3.49589	-4.40984	713.587
	8	668.049	0.000801617	3.5047	-4.43195	714.816
	9	1283.77	0.0000889697	3.51181	-4.4498	715.782
	10	2508.23	8.88926 × 10 ⁻⁶	3.51766	-4.46452	716.56*

PLL: profile log-likelihood

Table 4(c): Tempered stable estimation results on Bitcoin daily returns (~six significant digits)

			c = 0.5 (NIG)		
	n	\hat{a}_n	\hat{b}_n	$\hat{\mu}_n$	$\hat{ heta}_n$	PLL
	0	1.69903	40.2719	3.4866	-4.3844	741.57
	0.5	2.18658	34.0606	3.60284	-4.6784	744.017
	1	2.95041	31.8517	3.75372	-5.06738	746.459
	1.5	4.037	30.6647	3.91344	-5.48857	748.356
	2	5.56725	30.0464	4.08646	-5.95593	749.25
type I	2.5	7.72111	29.8558	4.27762	-6.48574	749.903
type i	3	10.7581	30.0452	4.49173	-7.09616	747.875
	3.5	15.0512	30.61	4.73399	-7.80857	750.611★
	4	21.1362	31.5722	5.01006	-8.64893	749.197
	4.5	29.7841	32.9755	5.32626	-9.64906	747.685
	5	42.1034	34.8824	5.68939	-10.8479	745.767
	n	\hat{a}_n	\hat{b}_n	$\hat{\mu}_n$	$\hat{ heta}_n$	PLL
	0	1.69903	40.2719	3.4866	-4.3844	741.57
	0.5	2.23523	35.6267	3.60867	-4.69302	744.468
	1	2.95041	31.8517	3.75372	-5.06738	746.459
	1.5	3.90955	28.8422	3.92845	-5.5294	748.107
	2	5.20409	26.5277	4.14219	-6.11131	748.78*
type II	2.5	6.96431	24.8739	4.40824	-6.86179	748.142
71	3	9.37804	23.891	4.74579	-7.85667	746.481
	3.5	12.7184	23.648	5.18271	-9.21738	747.08
	4	17.3826	24.2981	5.75891	-11.1428	743.584
	4.5	23.9386	26.1153	6.52903	-13.9616	739.578
	5	33.1604	29.5378	7.56059	-18.2114	731.809
	n	\hat{a}_n	\hat{b}_n	$\hat{\mu}_n$	$\hat{ heta}_n$	PLL
	0	1.69903	40.2719	3.4866	-4.3844	741.57
	0.5	2.14646	37.2922	3.62438	-4.73348	743.909
	1	2.95041	31.8517	3.75372	-5.06738	746.459
	1.5	4.19843	23.7357	3.84507	-5.30685	748.233
	2	6.13874	15.7484	3.9114	-5.48266	748.608
type III	2.5	9.19582	9.4846	3.96141	-5.61627	749.061
71	3	14.0854	5.26192	4.00036	-5.72095	749.327
	3.5	22.0249	2.71928	4.03151	-5.80506	749.486
	4	35.1087	1.32035	4.05697	-5.87407	749.581
	4.5	56.9807	0.606458	4.07815	-5.93167	749.634
	5	94.0523	0.264957	4.09606	-5.98048	749.657*

NIG: normal inverse Gaussian | PLL: profile log-likelihood

Table 4(d): Tempered stable estimation results on Bitcoin daily returns (~six significant digits)

			c=0.	75		
	n	\hat{a}_n	\hat{b}_n	$\hat{\mu}_n$	$\hat{ heta}_n$	PLL
	0	0.304774	50.5501	5.21772	-9.19796	752.733★
	0.1	0.321949	48.3428	5.26152	-9.33471	752.507
	0.2	0.341336	47.5163	5.34882	-9.6086	752.06
	0.3	0.362624	47.2887	5.4522	-9.9359	751.546
	0.4	0.385726	47.3793	5.56273	-10.2896	750.975
type I	0.5	0.410649	47.664	5.67699	-10.6595	750.398
type i	0.6	0.437445	48.0803	5.79359	-11.0415	749.811
	0.7	0.466199	48.594	5.91194	-11.434	749.224
	0.8	0.497011	49.1848	6.03186	-11.8366	748.614
	0.9	0.530001	49.8404	6.1533	-12.2493	748.005
	1	0.565299	50.5528	6.27632	-12.6725	747.39
	n	\hat{a}_n	\hat{b}_n	$\hat{\mu}_n$	$\hat{ heta}_n$	PLL
	0	0.304774	50.5501	5.21772	-9.19796	752.733★
	0.1	0.324226	50.3274	5.30404	-9.46608	752.302
	0.2	0.344917	50.1521	5.39414	-9.74882	751.851
	0.3	0.366924	50.0249	5.48823	-10.0472	751.379
	0.4	0.39033	49.9464	5.5865	-10.3622	750.885
type II	0.5	0.41522	49.9176	5.68916	-10.695	750.367
- J F	0.6	0.441685	49.9393	5.79643	-11.0469	749.825
	0.7	0.469821	50.0124	5.90855	-11.4192	749.257
	8.0	0.499731	50.1382	6.02574	-11.8131	748.663
	0.9	0.531519	50.3179	6.14824	-12.2304	748.041
	1	0.565299	50.5528	6.27632	-12.6725	747.39
	n	\hat{a}_n	\hat{b}_n	$\hat{\mu}_n$	$\hat{ heta}_n$	PLL
	0	0.304774	50.5501	5.21772	-9.19796	752.733★
	0.1	0.316506	49.8956	5.27563	-9.37895	752.433
	0.2	0.331647	50.6222	5.38789	-9.73239	751.857
	0.3	0.349699	51.6632	5.51481	-10.1368	751.21
	0.4	0.370556	52.6039	5.64265	-10.5493	750.562
type III	0.5	0.394296	53.2529	5.76595	-10.9521	749.939
71	0.6	0.421103	53.5212	5.88255	-11.3377	749.352
	0.7	0.451243	53.3751	5.99177	-11.7029	748.805
	8.0	0.485048	52.815	6.09357	-12.0468	748.297
	0.9	0.522912	51.8624	6.18827	-12.3697	747.826
	1	0.565299	50.5528	6.27632	-12.6725	747.39

PLL: profile log-likelihood

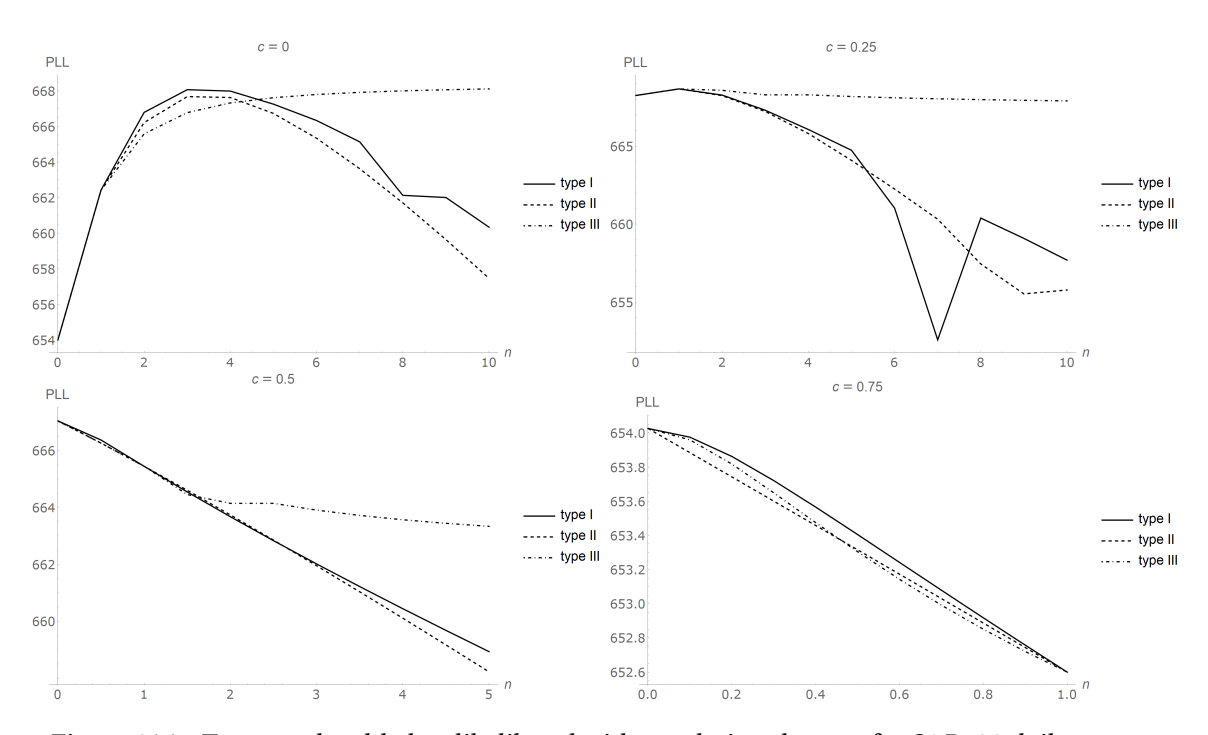


Figure 6(a): Tempered stable log-likelihood with regulation degrees for S&P500 daily returns

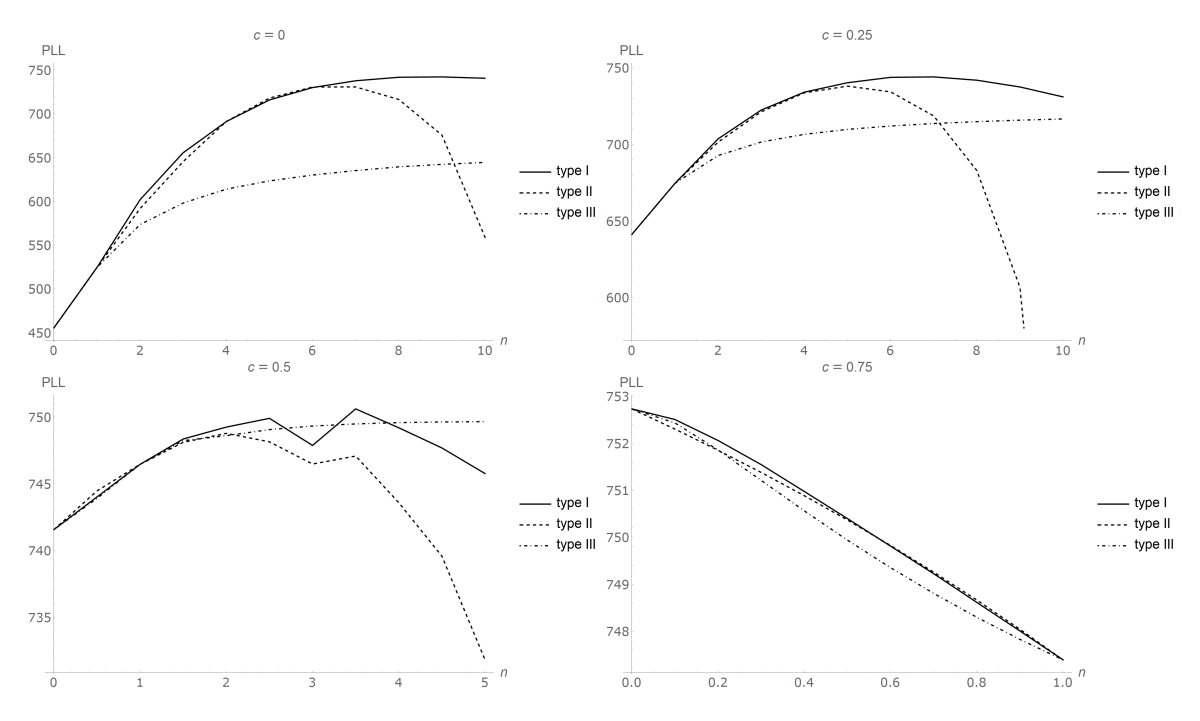


Figure 6(b): Tempered stable log-likelihood with regulation degrees for Bitcoin daily returns

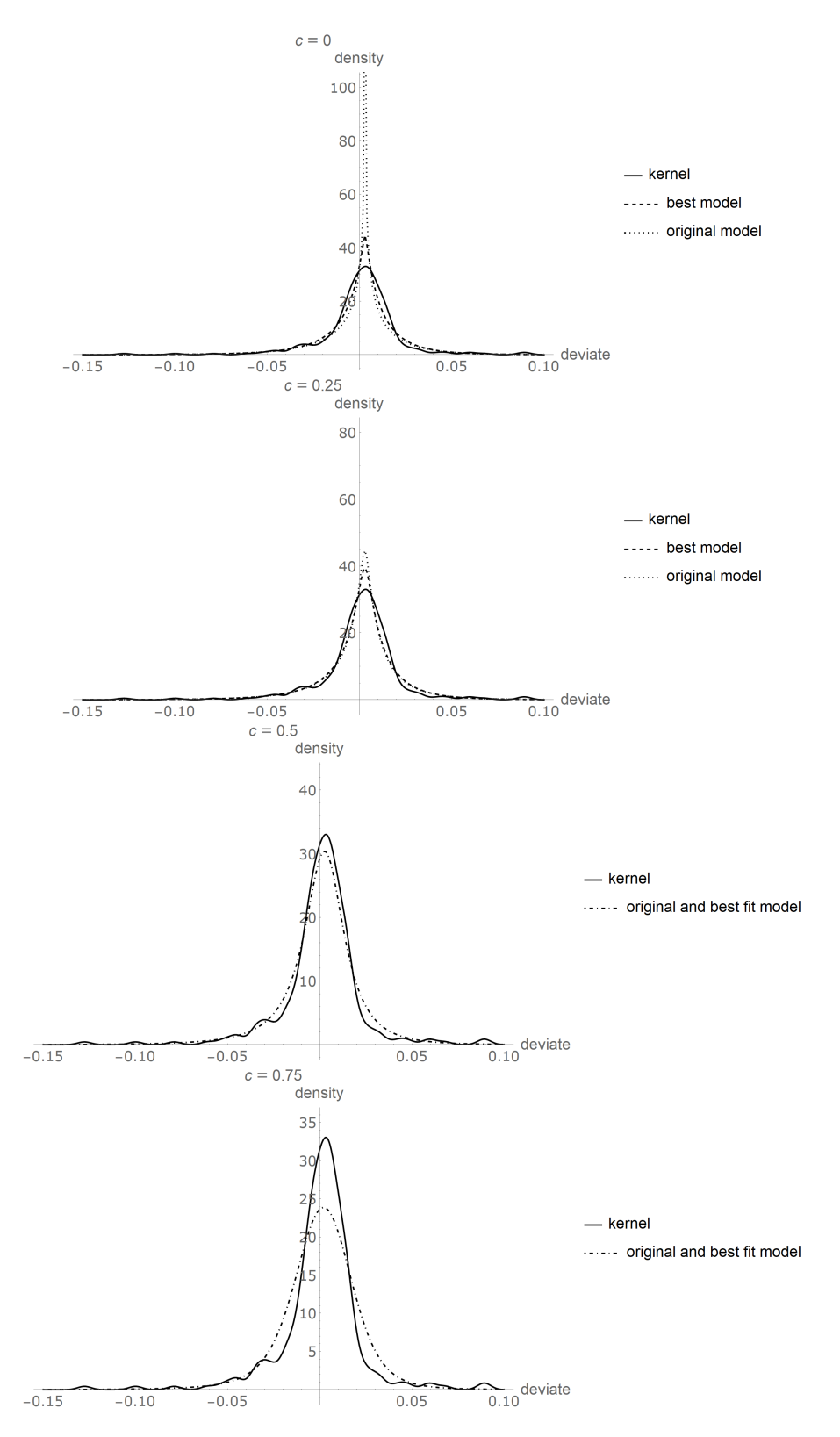


Figure 7(a): Tempered stable estimated densities with regulation degrees for S&P500 daily returns

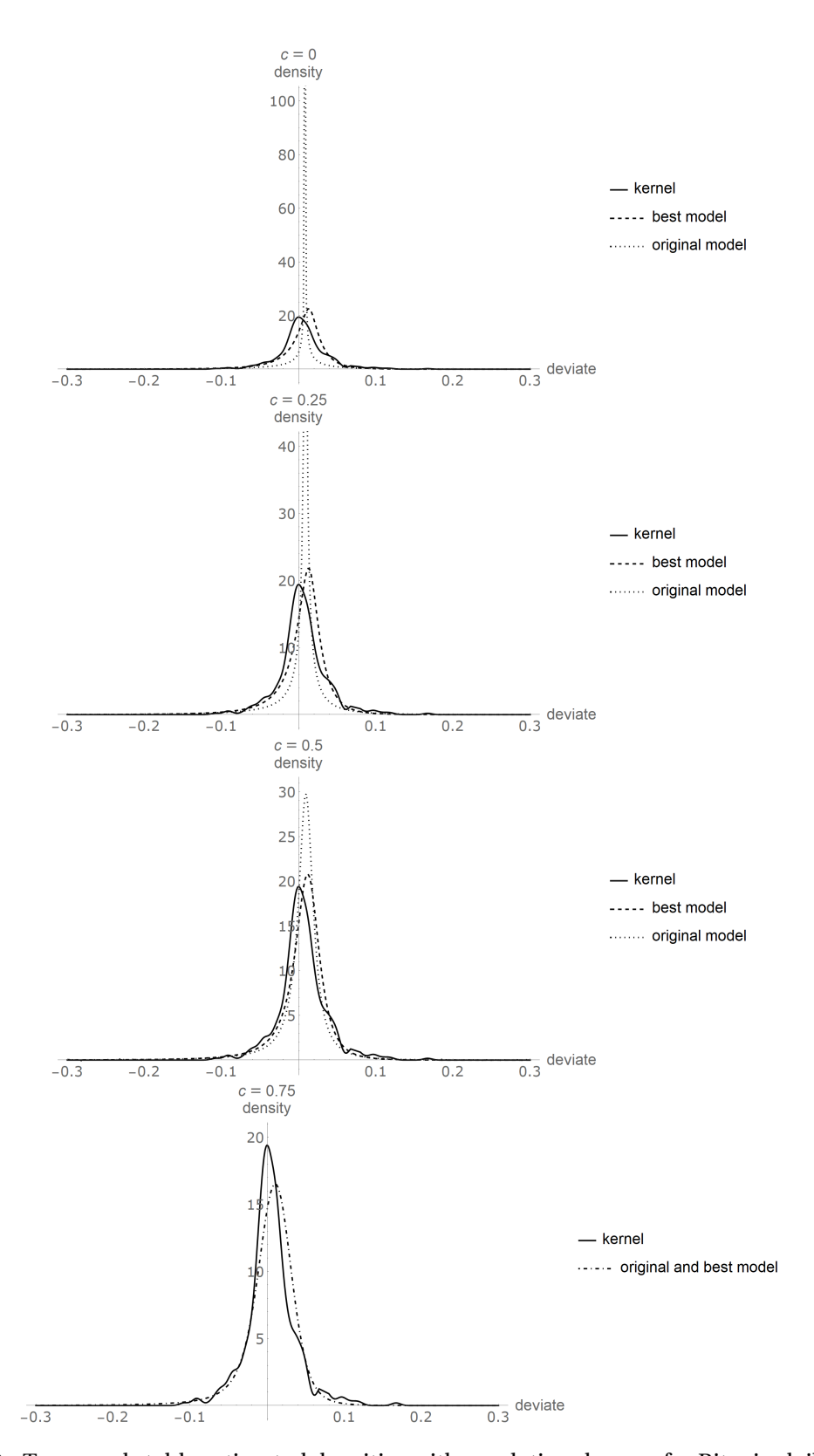


Figure 7(b): Tempered stable estimated densities with regulation degrees for Bitcoin daily returns

For the first exercise involving jump-diffusion models, from Table 2(a) and Table 2(b), the steady changes in the parameter values are clear for both data sets, which show robustness of the moment-based estimation. Specifically, while the estimate of the drift parameter, $\hat{\mu}_n$, has only marginally increased and that of the Brownian dispersion parameter, $\hat{\sigma}_n$, remains fairly stable, the infinite-divisibility parameter estimate $\hat{\lambda}_n$ has increased geometrically with the degree n regardless of the regulation type. This is in keeping with our original motivation to not reduce the measure of the number of trades. While decreasing, the rate of change of the rate parameter estimate \hat{b}_n , on the other hand, does depend on the regulation type, and is the lowest under the type I, moderate under the type II, and the highest (actually in orders of reciprocal factorials) under the type III. This is because the rate parameter plays the role of adjusting the local movement sizes of stochastic clocks in consonance with the decreasing effect from regulation. Speaking of the profile log-likelihood, we see that any type of regulation has resulted in a notable improvement for some $n \ge 1$. While the first two types tend to achieve a maximal value relatively quickly for $n \le 10$, the type III seems to be increasing the likelihood much more slowly. A simple explanation is that the third type has the mildest enlargement effect on distributional asymmetry and tail heaviness among the three. Besides, for both data sets the best models (with a "*") have all outperformed their counterparts with exponentially distributed jumps, also implying that jump-diffusion models with distorted uniformly distributed jump amplitudes can be used as an ideal replacement of the widely accepted exponential jump-diffusion models in most applications. The density plots in Figure 5 mainly show that despite closeness of the three estimated model densities, the peak of the one of the best fit model tends to lie between those of the models with uniform or exponential jumps, confirming its balancing characteristic mentioned in Subsection 4.1.

For the second exercise with Gaussian-mixed tempered stable models, it is seen from Table 3(a), Table 3(b), Table 3(c), Table 3(d), Table 4(a), Table 4(b), Table 4(c), and Table 4(d) that the parameter estimates also change steadily with the regulation degree, for all regulation types and both data sets. For any chosen value of the family parameter c and any regulation type, apart from marginal increases in the location parameter estimate $\hat{\mu}_n$ and the absolute Brownian drift estimate $|\hat{\theta}_n|$, the conspicuous value increase of the estimate \hat{a}_n of the infinite-divisibility parameter shows that clock regulation is indeed able to cater to a large number of trades while maintaining a significant level of asymmetry and tail heaviness. In the meantime, the interpretation of the value change of the rate parameter estimate \hat{b}_n is the same as in the jump-diffusion case in the first exercise. Viewing from the profile log-likelihood, the effect of regulation deteriorates rapidly as c increases, with the variance gamma case (c = 0) undergoing the greatest improvement. This phenomenon is within expectation, because in the limit as $c \nearrow 1$ the tempered stable subordinator will approach the usual drift clock of calendar time, which is by no means affected by regulation (or path averaging); equivalently, its Gaussian mixture will tend to a drifted Brownian motion, by the central limit theorem. ¹⁴ Such a trend is more salient for the S&P500 returns than for the Bitcoin returns, depending on the relative extent of asymmetrical and tail risks. To be fair, an intriguing observation is that by increasing the degree n of regulation the same level of loglikelihood (distributional information) has been achieved, whichever c-value is being used. Since c has an important dynamical meaning in terms of the local regularity of sample paths, and hence long-term trading intensity (recalling Section 1), clock regulation has therefore introduced a useful

 $^{^{14}}$ When minute-level data are employed, the value of c will probably be near 1 for liquid assets (see [Todorov and Tauchen, 2011, Table 5] [62]), in which case the underlying stochastic clock is close to the calendar time. This in turn shows that clock regulation is particularly useful for daily or lower-frequency data, making up their deficiency relative to the high-frequency counterparts which inevitably come at additional costs.

dimension for parameter estimation of a tempered stable model for any fixed value of the family parameter c. The fundamental difference, as we shall restate, is that the regulation degree n only changes the sizes of local movements and does not affect the Blumenthal–Getoor index (Corollary 1). The density plots in Figure 7(a) and Figure 7(b) further confirm the benefits of increasing the value of a (a large number of trades), as the original model density without clock regulation seems overly "peaked" (almost degenerate, or near trading halts) when its moments are matched to the empirical, while proper clock regulation helps get rid of such degeneracy tendency.

To demonstrate the method outlined in Subsection 5.2, we also do a calibration exercise on Bitcoin options using the Gaussian-mixed tempered stable models. The data set is directly taken from [Xia, 2021, Sect. 4.2] [68] and consists of M=40 Bitcoin call option prices quoted as of July 11th, 2020. The strike prices K range from \$3,000 to \$32,000 and there are four maturities: T=19,47,166,257 days. At the time of quoting, the Bitcoin price stood at $S_0=\$9,232.98$. We have q=r=0 for digital assets. To keep the demonstration concise, we also only consider four values of the family parameter $c \in \{0,0.25,0.5,0.75\}$ and choose the domain of regulation degrees $\mathfrak{N}=\{0,1,2,3,4,5\}$ (with $|\mathfrak{N}|=6$), which already give rise to 48 independent models. Each model is calibrated according to (5.2.2).

Table 5(a): Calibration results on Bitcoin options (~six significant digits)

type II									
	n	\hat{a}_n	\hat{b}_n	$\hat{ heta}_n$	MAPE (%)	CPU time (sec)			
c = 0 (VG)	0	52.8148	97.315	1.00541	24.7965	213.984			
	1	69.312	63.5709	0.835575	24.423	221.781			
	2	79.9247	34.5063	-0.0841175	24.368	1208.5			
	3	99.9403	21.5024	-0.271352	24.2491	1011.41			
	4	99.8584	10.7058	-0.806309	23.7375	2647.44			
	5	99.9986	5.30486	-1.21115	23.3089*	3961.56			
	n	\hat{a}_n	\hat{b}_n	$\hat{ heta}_n$	MAPE (%)	CPU time (sec)			
c = 0.25	0	5.29036	24.9255	-1.4834	22.5461	347.219			
	1	5.55635	9.93689	-1.70271	20.484	501.266			
	2	6.89235	5.1679	-1.64386	21.5499	3029.7			
	3	2.81083	0.476929	-1.48728	19.065*	13629.9			
	4	-	-	-	-	-			
	5	-	-	-	-	-			
	n	\hat{a}_n	\hat{b}_n	$\hat{ heta}_n$	MAPE (%)	CPU time (sec)			
	0	0.485557	1.37746	-1.59762	19.2856	135.625			
	1	0.664932	0.572124	-1.46531	19.2146	378.313			
c = 0.5	2	1.03635	0.343634	-1.44776	19.1939*	618.609			
(NIG)	3	-	-	-	-	-			
(112)	4	-	-	-	-	-			
	5	-	-	-	-	-			
	n	\hat{a}_n	\hat{b}_n	$\hat{ heta}_n$	MAPE (%)	CPU time (sec)			
c = 0.75	0	0.288703	9.88632	-1.18918	23.3422	164.516			
	1	0.331241	0.608326	-1.32828	20.6779*	304.75			
	2	-	-	-	-	-			
	3	-	=	-	-	-			
	4	-	-	-	-	-			
	5	-	-	-	-	-			

MAPE: mean absolute percentage error | VG: variance gamma | NIG: normal inverse Gaussian

Table 5(b): Calibration results on Bitcoin options (~six significant digits)

type III							
	n	\hat{a}_n	\hat{b}_n	$\hat{ heta}_n$	MAPE (%)	CPU time (sec)	
c = 0 (VG)	0	52.8148	97.315	1.00541	24.7965	213.984	
	1	69.312	63.5709	0.835575	24.423	221.781	
	2	25.7893	7.01917	-1.82847	21.9319*	1386.55	
	3	80.8854	5.83995	-0.551056	23.9882	1071.81	
	4	90.3674	1.28759	-0.786714	23.8168	968.281	
	5	97.9971	0.232557	-0.926549	23.6565	764.641	
	n	\hat{a}_n	\hat{b}_n	$\hat{ heta}_n$	MAPE (%)	CPU time (sec)	
c = 0.25	0	5.29036	24.9255	-1.4834	22.5461	347.219	
	1	5.55635	9.93689	-1.70271	20.484	501.266	
	2	4.40503	1.49887	-1.62404	18.5857*	1442.34	
	3	7.26858	0.477655	-1.8991	19.6144	673.453	
	4	9.61409	0.0816453	-1.64024	18.9021	681.328	
	5	9.94952	0.0053706	-2.12896	24.8041	1469.98	
	n	\hat{a}_n	\hat{b}_n	$\hat{ heta}_n$	MAPE (%)	CPU time (sec)	
c = 0.5	0	0.485557	1.37746	-1.59762	19.2856	135.625	
	1	0.664932	0.572124	-1.46531	19.2146	378.313	
	2	1.30094	0.242459	-1.45114	19.1893*	492.594	
(NIG)	3	3.02094	0.0752527	-1.54985	19.2294	1282.11	
(-1)	4	9.89913	0.0457464	-1.59855	19.9204	815.641	
	5	9.95359	0.0000857145	-1.25003	23.4282	1602.34	
	n	\hat{a}_n	\hat{b}_n	$\hat{ heta}_n$	MAPE (%)	CPU time (sec)	
c = 0.75	0	0.288703	9.88632	-1.18918	23.3422	164.516	
	1	0.331241	0.608326	-1.32828	20.6779	304.75	
	2	0.978496	0.728833	-1.24462	22.117	762.734	
	3	1.82492	0.00378187	-1.30428	19.4049*	750.078	
	4	6.33734	0.000522405	-1.31269	19.43	708.563	
	5	27.7777	0.000615278	-1.37646	19.8326	903.156	

MAPE: mean absolute percentage error | VG: variance gamma | NIG: normal inverse Gaussian

As discussed in Subsection 5.2, the optimal parameter values are subject to minor instability with joint calibration. For this reason, the main goal of this calibration exercise is to demonstrate that tempered stable models with clock regulation can be used with high efficiency and well expected to outperform the originals with unregulated clocks for financial derivatives valuation. The calibration results are summarized in Table 5(a) and Table 5(b), along with (locally) minimal pricing error and CPU time (with only a quad-core processor). Notably, under type-II regulated clocks, since the computational complexity of the formula (4.2.1) can increase rapidly with the degree of regulation, some models for c > 0 and $n \ge 2$ have not been successfully calibrated within a reasonable time limit (24 hours), and hence their results have been deliberately left out for comparability, while the remaining results are sufficient to serve our conclusions. Likewise, for each chosen value of c, the model with the best fit is marked "*."

From Table 5(a) and Table 5(b) we can see that adopting regulated clocks has significantly improved the calibration results, regardless of the value of c. More specifically, for type-II regulation, better performance is generally produced by increasing n, though the computation time grows drastically simultaneously. The latter feature is especially notable if c > 0, when one is forced to apply (4.2.1) outside the unit disk, whereas for the variance gamma model with c = 0, the more

elementary formula (4.2.2) is used instead. In contrast, under type-III regulation, computation time does not scale with the degree of regulation, but there is oftentimes an optimal value n < 5 that gives a best fit.

Speaking of the optimized parameter values, we observe that, for each fixed value of c, \hat{a}_n usually increases with n while \hat{b} decreases, which is similar to the results of statistical estimation. Besides, $\hat{\theta}_n$ seems to be very stable in general, implying, yet again, that the Brownian drift parameter is largely uninfluenced by clock regulation. From Table 5(a) and Table 5(b) we identify the best fit model as the one with c = 0.25 and n = 2 under type-III regulation, whose implied prices are further visually compared with the market prices in Figure 8.

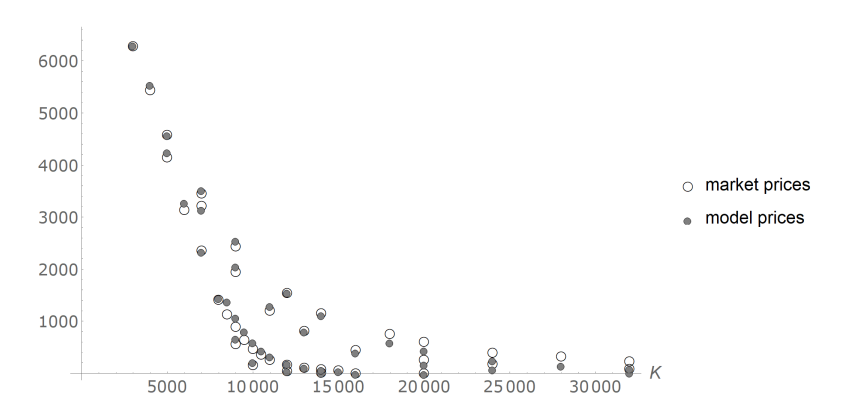


Figure 8: Bitcoin option prices (market vs best fit model)

Furthermore, we compare in Figure 9 the risk-neutral densities (namely the Q-densities) of annualized Bitcoin log-returns (driven by $\Xi_1^{(n),Z}$ for $n\in\mathbb{N}\cap[0,5]$) to further illustrate the static effect of clock regulation, though for succinctness the illustration is only done for the subcase "type III, c=0.25" of which the best fit model is a special case. The formula (4.2.7) is applied because c<1/2, along with the choice $\mu_n=-\log\phi_{\Xi_1^{(n),Z}}(-1)$.

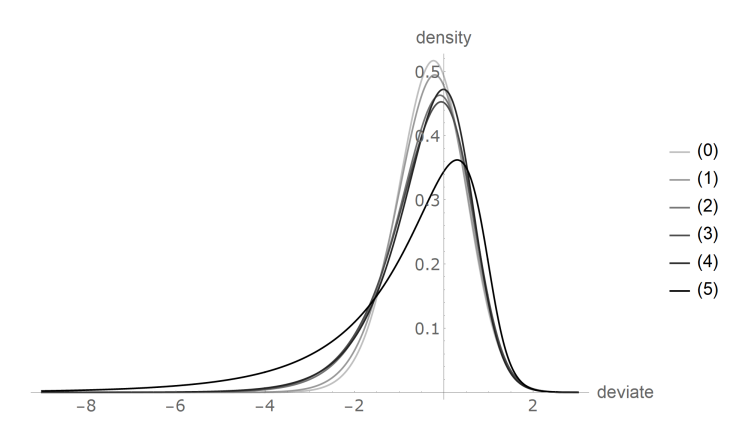


Figure 9: Option-implied risk-neutral densities of Bitcoin log-returns (type III, c = 0.25)

7 Concluding remarks

In this paper we have studied the regulation of stochastic clocks built from Lévy subordinators for the purpose of tackling asymmetrical and tail risks typically observed in financial returns without making undesirable changes on parameters linked to important aspects of the trading activity. These parameters are those measuring infinite divisibility or α -stability and so making such an improvement has potential not only in enhancing capacity of the original processes but in balancing various modeling emphases involving the microstructure of data as well. From the viewpoint of static distributions, a direct effect is to arbitrarily enlarge skewness and (excess) kurtosis, while being able to fix the mean and variance and not decrease the jump intensity (or approach degeneracy).

The methodology comes in three concrete recipes. Despite a common motivation from repeated continuous-time averaging, the recipes vary in their impact on the original distributional asymmetry and tail heaviness as well as the computational complexity of resultant distribution formulae, which properties are summarized and compared in Table 6 for the convenience of the reader.

Category	type I	type II	type III				
induction nature	average of sample paths	average of log-LT	quasi-average of				
muuchon nature	average of sample paths	average of log-L1	sample paths				
regulating kernel	incomplete gamma	inverse gamma	Riemann-Liouville				
Lévy measure distortion	severe	moderate	mild				
Skew/EKurt enlargement	faster than exponential	exponential	slower than linear				
Skew/Ekurt emargement	laster than exponential	ехропенна	or bounded				
explicit formulae	LT: $n = 1$ only	LT: $n \in \mathbb{N}_{++}$ only	IT and I M. any n > 0				
(Poisson)	LM: any $n > 0$	LM: any $n > 0$	LT and LM: any $n > 0$				
explicit formulae	IT and IM: n = 1 only	LT and LM: $n \in \mathbb{N}_{++}$	LT and LM: any $n > 0$				
(tempered stable)	LT and LM : $n = 1$ only	LI allu Livi. $n \in \mathbb{N}_{++}$					
IT: I and a set the section of I M. I for the account							

Table 6: Summary of properties of regulated stochastic clocks

LT: Laplace transform | LM: Lévy measure

Generally speaking, stochastic clock regulation works well on any Lévy subordinator as long as the prerequisite (2.1) of generic-time log-LT analyticity is satisfied and can be utilized to obtain a good number of newfangled Lévy models for financial modeling and other uses. It is only futile for processes whose generic-time log-LT is linear or undefined in the neighborhood of zero. ¹⁵ Clearly, in the former case the subordinator is degenerate and effectively identical to the clock of calendar time, and in the latter it does not have a finite third-order cumulant. The resultant mixed models then have skewness and excess kurtosis either equal to zero or undefined (including infinity) – obviously, both zero and infinity cannot be further "enlarged" by multiplication.

When applied to a Poisson process, the regulated clocks have led to compound Poisson processes with bounded jumps having a truncated exponential-like distribution and hence corresponding jump—diffusion models inheriting the advantages of both the uniform distribution ([Yan and Hanson, 2006] [69]) and the (usual) exponential distribution ([Kou, 2002] [40]). As our empirical study on S&P500 and Bitcoin returns has shown, when moment-based estimation is employed

 $^{^{15}}$ Note that the log-LT cannot be a finite-order polynomial of degree greater than two; see [Lukacs, 1970, Thm. 7.3.5] [45].

to match the empirical skewness and kurtosis, the profile likelihood for the new models with regulation degree n > 0 is indeed improved relative to the uniform and the pure-exponential, which signifies that the distorted uniform distributions are suitable for modeling downside risks in a jump–diffusion framework.

Secondly, operating the regulated clocks on the Gaussian-mixed tempered stable models generates a series of modified processes with unchanged path regularity but enhanced distributional asymmetry and tail heaviness. The empirical results imply that the effect of regulation is most conspicuous when the family parameter c is small, close to the case of variance gamma processes, while it gradually diminishes as c approaches the upper limit 1, when the mixed model tends to Gaussianity. More importantly, by varying the degree n of regulation, one can expect to easily take account of empirical skewness and kurtosis of returns without losing essential information on the actual distribution, regardless of which value of c is in use. Put differently, in the presence of the hyperparameter n, the value of c can be confidently fixed for a certain data frequency or taken from other sources of estimation, since n, benignly, has no effect on the local regularity of the stochastic process.

The methodology that the present paper has put forward is a jump-off point and so can be advanced in various directions. For instance, as we have mentioned since Section 1, it can be extended to subordinators of the Sato type (with non-stationary increments) with reasonable effort as well as the establishment of mean-reverting time changes of Ornstein-Uhlenbeck type ([Carr and Wu, 2004 [19]) for stochastic volatility. Also, an ongoing research is concerned with developments into a multidimensional setting, especially for the Gaussian mixed models, which will be conducive to portfolio analysis and derived optimization problems. We note that multivariate subordination of Brownian motion via tempered stable subordinators has received much attention in the literature; see, e.g., [Luciano and Semeraro, 2010a] [43], [Luciano and Semeraro, 2010b] [44], [Pérez-Abreu and Stelzer, 2014] [53], and [Mandoza-Arriaga and Linetsky, 2016] [48]. Of course, the two special cases discussed in Section 4 are also far from exhaustive, and it is possible to consider operating the regulating kernels on other choices of Lévy subordinators, e.g., compound Poisson-exponential processes or generalized inverse Gaussian processes ([Barndorff-Nielsen and Halgreen, 1977 [8]), and derive the moment-based estimation procedures in the same spirit as in Subsection 5.1. Last but not least, the empirical aspect may be strengthened by studying other kinds of financial time series, such as individual stocks, exchange rates, volatility indices, etc., in order to explore how the degree of clock regulation is fundamentally reflected in trading volumes or relative illiquidity and its variation with different levels of asymmetrical and tail risks.

References

- [1] Abramowitz, M., Stegun, I.A. *Handbook of Mathematical Functions with Formulas, Graphs, and Mathematical Tables*, 10th Printing, U.S. National Bureau of Standards, Washington, D.C., 1972.
- [2] Aguilar, J-P., Kirkby, J.L., Korbel, J. (2020). Pricing, risk and volatility in subordinated market models. *Risks*, 8: No. 124.
- [3] Aït-Sahalia, Y., Jacod, J. (2009). Testing for jumps in a discretely observed process. Annals of Statistics, 37: 184-222.
- [4] Alexander, G.J., Peterson, M.A. (2007). An analysis of trade-size clustering and its relation to stealth trading. *Journal of Financial Economics*, 84: 435–471.

- [5] Ané, T., Geman, H. (2000). Order flow, transaction clock, and normality of asset returns. *Journal of Finance*, 55: 2259–2284.
- [6] Bandi, F.M., Nguyen, T.H. (2003). On the functional estimation of jump–diffusion models. *Journal of Econometrics*, 116: 293–328.
- [7] Barndorff-Nielsen, O.E. (1997). Normal inverse Gaussian distributions and stochastic volatility models. Scandinavian Journal of Statistics, 24: 1–13.
- [8] Barndorff-Nielsen, O.E., Halgreen, C. (1977). Infinitely divisibility of the hyperbolic and generalized inverse Gaussian distributions. *Zeitschrift für Wahrscheinlichkeitstheorie und verwandte Gebiete*, 38: 309–311.
- [9] Barndorff-Nielsen, O.E., Pollard, D.G., Shephard, N. (2011). Integer-valued Lévy processes and low latency financial econometrics. *Quantitative Finance*, 12: 587–605.
- [10] Bateman, H. Tables of Integral Transforms, 1st Vol., McGraw-Hill, New York-Toronto-London, 1954.
- [11] Bateman, H., Erdélyi, A. Higher Transcendental Functions, 2nd Vol., McGraw-Hill, New York, 1954.
- [12] Baustian, F., Mrázek, M., Pospíšil, J., Sobotka, T. (2017). Unifying pricing formula for several stochastic volatility models with jumps. *Applied Stochastic Models in Business and Industry*, 33: 422–442.
- [13] Beckers, S. (1981). A note on estimating the parameters of the diffusion–jump model of stock returns. *Journal of Financial and Quantitative Analysis*, 16: 127–140.
- [14] Blau, B.M. (2017). Price dynamics and speculative trading in bitcoin. *Research in International Business and Finance*, 41: 493–499.
- [15] Blumenthal, R.M., Getoor, R.K. (1961). Sample functions of stochastic processes with stationary independent increments. *Journal of Mathematics and Mechanics*, 10: 493–516.
- [16] Bollerslev, T. (1987). A conditionally heteroskedastic time series model for speculative prices and rates of return. *Review of Economics and Statistics*, 69: 542–547.
- [17] Boyarchenko, S.I., Levendorskii, S.Z. (2000). Option pricing for truncated Lévy processes. *International Journal of Theoretical and Applied Finance*, 3: 549–552.
- [18] Carr, P., Gemen, H., Madan, D.B., Yor, M. (2002). The fine structure of asset returns: An empirical investigation. *The Journal of Business*, 75: 305–332.
- [19] Carr, P., Wu, L. (2004). Time-changed Lévy processes and option pricing. *Journal of Financial Economics*, 71: 113–141.
- [20] Chaim, P., Laurini, M.P. (2019). Nonlinear dependence in cryptocurrency markets. *North American Journal of Economics and Finance*, 48: 32–47.
- [21] Chang, E.C., Pinegar, J.M., Schachter, B. (1997). Interday variations in volume, variance and participation of large speculators. *Journal of Banking and Finance*, 21: 797–810.
- [22] Chen, T. (2019). The price impact of trade-size clustering: Evidence from an intraday analysis. *Journal of Business Research*, 101: 300–314.
- [23] Clark, P.K. (1973). A subordinated stochastic process model with finite variance for speculative prices. Econometrica, 41: 135–155.
- [24] DiDonato, A.R., Morris, A.H. (1986). Computation of the incomplete gamma function ratios and their inverse. *ACM Transactions on Mathematical Software*, 12: 377–393.
- [25] Downton, F. (1972). The area under the infectives trajectory of the general stochastic epidemic. *Journal of Applied Probability*, 9: 414–417.

- [26] Eberlein, E., Madan, D.B. (2009). Sato processes and the valuation of structured products. *Quantitative Finance*, 9: 27–42.
- [27] Fallahgoul, H., Loeper, G. (2021). Modelling tail risk with tempered stable distributions: An overview. Annals of Operations Research, 299: 1253–1280.
- [28] Geman, H. Stochastic clock and financial markets. In: Aspects of Mathematical Finance, Springer, Berlin, Heidelberg, 37–52, 2008.
- [29] Geman, H., Madan, D.B., Yor, M. (2001). Time changes for Lévy processes. Mathematical Finance, 11: 79–96.
- [30] Gkillas, K., Katsiampa, P. (2018). An application of extreme value theory to cryptocurrencies. *Economics Letters*, 164: 109–111.
- [31] Grabchak, M. (2021). Discrete tempered stable distributions. *Methodology and Computing in Applied Probability*, Online First, 1–14.
- [32] Gradshteyn, I.S., Ryzhik, I.M. *Table of Integrals, Series, and Products*, 7th Ed. Academic Press, Elsevier, Burlington, 2007.
- [33] Gupta, N., Kumar, A., Leonenko, N.N. (2020). Skellam type processes of order k and beyond. Entropy, 22: 1193.
- [34] Jing, B-Y., Kong, X-B., Liu, Z., Mykland, P. (2012). On the jump activity index for semimartingales. *Journal of Econometrics*, 166: 213–223.
- [35] Jondeau, E., Rockinger, M. (2003). Conditional volatility, skewness, and kurtosis: Existence, persistence, and comovements. *Journal of Economic Dynamics and Control*, 27: 1699–1737.
- [36] Kalmykov, M.Y., Kniehl, B.A. (2009). Towards all-order Laurent expansion of generalised hypergeometric functions about rational values of parameters. *Nuclear Physics B*, 809 [PM]: 365–405.
- [37] Karpoff, J.M. (1987). The relation between price changes and trading volume: A survey. *Journal of Financial and Quantitative Analysis*, 22: 109–126.
- [38] Kerss, A., Leonenko, N.N., Sikorskii, A. (2014). Fractional Skellam processes with applications to finance. *Fractional Calculus & Applied Analysis*, 17: 532-551.
- [39] Koponen, I. (1995). Analytic approach to the problem of convergence of truncated Lévy flights towards the Gaussian stochastic process. *Physical Review E*, 52: 1197–1199.
- $[40] \ \ Kou, S.\ (2002).\ A\ jump-diffusion\ model\ for\ option\ pricing.\ \textit{Management Science},\ 48:\ 1086-1101.$
- [41] Küchler, U., Tappe, S. (2013). Tempered stable distributions and processes. *Stochastic Processes and their Applications*, 123: 4256–4293.
- [42] Liu, Y., Tsyvinski, A. (2021). Risks and returns of cryptocurrency. The Review of Financial Studies, 34: 2689–2727.
- [43] Luciano, E., Semeraro, P. (2010a). A generalized normal mean–variance mixture for return processes in finance. *International Journal of Theoretical and Applied Finance*, 13: 415–440.
- [44] Luciano, E., Semeraro, P. (2010b). Multivariate time changes for Lévy asset models: Characterization and calibration. *Journal of Computational and Applied Mathematics*, 233: 1937–1953.
- [45] Lukacs, E. Characteristic Functions, 2nd Ed., Griffin, London, 1970.
- [46] Madan, D.B., Carr, P., Chang, E.C. (1998). The variance gamma process and option pricing. *European Finance Review*, 2: 79–105.
- [47] Madan, D.B., Reyners, S., Schoutens, W. (2019). Advanced model calibration on bitcoin options. *Digital Finance*, 1: 117–137.

- [48] Mandoza-Arriaga, R., Linetsky, V. (2016). Multivariate subordination of Markov processes with financial applications. Mathematical Finance. 26: 699–747.
- [49] Mittnik, S., Paolella, M.S., Rachev, S.T. (2000). Diagnosing and treating the fat tails in financial returns data. *Journal of Empirical Finance*, 7: 389–416.
- [50] Monroe, I. (1978). Processes that can be embedded in Brownian motion. Annals of Probability, 6: 42-56.
- [51] Ornthanalai, C. (2014). Lévy jump risk: Evidence from options and returns. Journal of Financial Economics, 112: 69–90.
- [52] Orsingher, E., Polito, F. (2013). On the integral of fractional Poisson processes. *Statistics and Probability Letters*, 83: 1006–1017.
- [53] Pérez-Abreu, V., Stelzer, R. (2014). Infinitely divisible multivariate and matrix gamma distributions. *Journal of Multivariate Analysis*, 130: 155–175.
- [54] Pollett, P.K. (2003). Integrals for continuous-time Markov chains. Mathematical Biosciences, 182: 213-225.
- [55] Richardson, M., Smith, T. (1994). A direct test of mixture distribution hypothesis: Measuring the daily flow of information. *Journal of Financial and Quantitative Analysis*, 29: 101–116.
- [56] Ronsiński, J. (2007). Tempering stable processes. Stochastic Processes and their Applications, 117: 677–707.
- [57] Samorodnitsky, G., Taqqu, M.S. Stable Non-Gaussian Random Processes: Stochastic Models with Infinite Variance. Chapman & Hall / CRC, New York, 1994.
- [58] Sato, K-I. (2006). Additive processes and stochastic integrals. Illinois Journal of Mathematics, 50: 825–851.
- [59] Schoutens, W. Lévy Processes in Finance: Pricing Financial Derivatives. The Atrium, Southern Gate, Chichestor: John Wiley & Sons Ltd, 2003.
- [60] Slater, L.J. Generalized Hypergeometric Functions, Cambridge University Press, Cambridge, UK, 1966.
- [61] Todorov, V. (2021). Nonparametric jump variation measures from options. Journal of Econometrics, Online First.
- [62] Todorov, V., Tauchen, G. (2011). Volatility jumps. Journal of Business and Economic Statistics, 29: 356–371.
- [63] Troster, V., Tiwari, A.K., Shahbaz, M., Macedo, D.N. (2019). Bitcoin returns and risk: A general GARCH and GAS analysis. *Finance Research Letters*, 30: 187–193.
- [64] Tseng, S-P., Peng, C-Y. (2004). Optimal burn-in policy by using an integrated Wiener process. *IIE Transactions*, 36: 1161–1170.
- [65] Van Noortwijk, J.M. (2009). A survey of the application of gamma processes in maintenance. *Reliability Engineering & System Safety*, 94: 2–21.
- [66] Wang, X., Xu, D. (2010). An inverse Gaussian process model for degradation data. Technometrics, 52: 188-197.
- [67] Xia, W. (2019). The average of a negative-binomial Lévy process and a class of Lerch distributions. *Communications in Statistics Theory and Methods*, 49: 1008–1024.
- [68] Xia, W. (2021). Average-tempered stable subordinators with applications. Applied Stochastic Models in Business and Industry, 37: 1097–1122.
- [69] Yan, G., Hanson, F.B. Option pricing for a stochastic-volatility jump–diffusion model with log-uniform jump-amplitude. In: *Proceedings of American Control Conference*, Minneapolis, MI, USA, June, 14–16, 2006.
- [70] Ye, Z-S., Xie, M. (2015). Stochastic modelling and analysis of degradation for highly reliable products. *Applied Stochastic Models in Business and Industry*, 31: 16–32.

Appendix A Mathematical proofs

Theorem 1

Proof. Let t > 0 be fixed. By applying integration-by-parts to (2.1.1) n times we have the fractional integral representation

$$\bar{X}_t^{(n)} = \frac{1}{t\Gamma(n)} \int_0^t X_s \log^{n-1} \frac{t}{s} ds = \int_0^t \left(1 - \frac{\Gamma(n, \log(t/s))}{\Gamma(n)} \right) dX_s, \tag{A.1}$$

where the second equality follows from the substitution $\log(t/s) \mapsto s$.¹⁶ The representation (A.1) together with the fact that X is a Lévy process allows to write

$$\mathsf{E} e^{-u\bar{X}_t^{(n)}} = \prod_{0}^t \mathsf{E} \Big(\exp\Big(-uX_1\Big(1 - \frac{\Gamma(n,\log(t/s))}{\Gamma(n)}\Big) \Big) \Big)^{\mathrm{d}s} = \exp\Big(\int_0^t \log \phi_{X_1}\Big(\Big(1 - \frac{\Gamma(n,\log(t/s))}{\Gamma(n)}\Big)u\Big) \mathrm{d}s \Big),$$

where \prod is the geometric integral sign and which leads to the first formula in (2.1.5) with the substitution $s/t \mapsto s$.

For the other two formulae it suffices to identify the corresponding fractional integral representations. For (2.1.3), observe that for each $n \ge 1$, $\tilde{X}^{(n)}$ is the running average of the given Lévy process $Y^{(n-1)}$, so that the LT of $\tilde{X}^{(n)}_t$ at generic time satisfies the recurrence relation

$$\phi_{\tilde{X}_t^{(n)}}(u) = \exp\left(\frac{t}{u} \int_0^u \log \phi_{\tilde{X}_1^{(n-1)}}(v) dv\right), \quad \text{Re} \, u \ge 0, \tag{A.2}$$

due to the independent increments property of $Y^{(n-1)}$. The recurrence can be resolved easily via integration-by-parts, given the initial condition $\tilde{X}^{(0)} \equiv X$, in the same vein as (A.1), yielding the second formula in (2.1.5).

Also, since the integrals in (2.1.4) are simply iterated, an application of Cauchy's repeated integration formula immediately gives

$$\check{X}_t^{(n)} = \frac{1}{t^n \Gamma(n+1)} \int_0^t (t-s)^n \mathrm{d}X_s,$$

which result shows that each $\check{X}^{(n)}$ can be treated as a (times-scaled) usual fractional Lévy process under the Riemann–Liouville kernel.

Theorem 2

Proof. Comparing the first formula in (2.1.5) with the first formula in (2.2.1), we obtain the following Fredholm integral equation:

$$\int_0^\infty (e^{-uz} - 1)\bar{v}^{(n)}(\mathrm{d}z) = \int_0^1 \int_0^\infty \left(e^{-(1 - \Gamma(n, -\log s)/\Gamma(n))uz} - 1 \right) \nu(\mathrm{d}z) \mathrm{d}s,$$

but as $1-\Gamma(n,-\log s)/\Gamma(n)\geq 0$ for all $n\geq 1$ and $s\in [0,1]$, the substitution $(1-\Gamma(n,-\log s)/\Gamma(n))z\mapsto z$ together with the Fubini–Tonelli theorem yields

$$\bar{v}^{(n)}(\mathrm{d}z) = \int_0^1 v \left(\mathrm{d} \frac{\Gamma(n)z}{\Gamma(n) - \Gamma(n, -\log s)} \right) \mathrm{d}s, \quad z \ge 0.$$
 (A.3)

¹⁶The first recipe generalizes the fractional integration of nonnegative processes to logarithmic kernels, as for every $n \ge 1$ and t > 0 the integrand $(1/(t\Gamma(n))X_s\log^{n-1}(t/s))_{s∈(0,t]}$ in (A.1) constitutes a nonnegative stochastic process.

Since $[0,1] \ni s \mapsto \Gamma(n)/(\Gamma(n) - \Gamma(n,-\log s)) \in [1,\infty)$ forms a strictly increasing function for each $n \ge 1$, we can apply the further substitution $\Gamma(n)/(\Gamma(n) - \Gamma(n,-\log s)) \mapsto y$ to obtain the first formula in (2.2.2), after some rearrangement.

Then, for each fixed $n \ge 1$, comparing the second formula in (2.1.5) with the second formula in (2.2.1) and interchanging integrals gives the following integral equation:

$$\int_0^\infty (e^{-uz} - 1)\tilde{v}^{(n)}(\mathrm{d}z) = \int_0^\infty \int_0^1 (e^{-uvz} - 1)\mathrm{d}v\tilde{v}^{(n-1)}(\mathrm{d}z),$$

which is equivalent, on rearranging the right-hand side, to

$$\int_0^\infty (e^{-uz} - 1)\tilde{v}^{(n)}(\mathrm{d}z) = \int_0^\infty (e^{-uz} - 1) \int_1^\infty \frac{\tilde{v}^{(n-1)}(\mathrm{d}(yz))}{v^2} \mathrm{d}y.$$

It leaves us with no choice but

$$\tilde{v}^{(n)}(\mathrm{d}z) = \int_{1}^{\infty} \frac{\tilde{v}^{(n-1)}(\mathrm{d}(yz))}{v^2} \mathrm{d}y.$$

This is yet another recurrence equation similar to the ones solved before, subject to the initial condition $\tilde{v}^{(0)} \equiv v$. Upon integration-by-parts we obtain the second formula in (2.2.2).

It is straightforward to obtain the third formula in (2.2.2) by mimicking the steps taken for the first.

With absolute continuity with respect to Lebesgue measure, the corresponding formulae for Lévy densities in (2.2.3) follow from direct calculations.

Corollary 1

Proof. According to the definition of the Blumenthal–Getoor index, it suffices to observe that the relations in (2.2.2) (or (2.2.3)) entail integration over domains bounded away from zero. Then the sigma-finiteness of the Lévy measures along with the Fubini–Tonelli theorem implies that the finiteness of the integrals $\int_0^1 |z|^p \tilde{v}^{(n)}(\mathrm{d}z)$, $\int_0^1 |z|^p \tilde{v}^{(n)}(\mathrm{d}z)$, and $\int_0^1 |z|^p \tilde{v}^{(n)}(\mathrm{d}z)$, for any n>0, are all equivalent to that of $\int_0^1 |z|^p v(\mathrm{d}z)$, for any p>0.

Corollary 2

Proof. Fix n > 0. The construction of the coefficients $C_{m,n}$ and $1/((mn+1)\Gamma^m(n+1))$, $m \in \mathbb{N}_{++}$, for the type I and type III, respectively, is a direct result of Theorem 1, or the fractional integral representations (A.1) and (A.2). For the type II, since induction takes place for each n, the coefficients $1/(m+1)^n$, $m \in \mathbb{N}_{++}$, are obtained by noting that $C_{m,1} = \int_0^1 (1-s)^m \mathrm{d}s = 1/(m+1)$.

The rationality of $C_{m,n}$'s is seen from the fact that, for every $n \in \mathbb{N}_{++}$, $\Gamma(n) \equiv (n-1)!$ and the finite series representation $\Gamma(n, -\log s) = (n-1)! s \sum_{k=0}^{n-1} (-\log s)^k / k!$, and $\int_0^1 s^j (-\log s)^k ds = k! / (j+1)^{k+1}$ for any $j,k \in \mathbb{N}$.

Corollary 3

Proof. The formulae follow immediately by replacing X with its regulated counterparts in (3.1.2).

Corollary 4

Proof. According to Corollary 1, it is enough to consider the constant mixture ξ^X based on the Lévy subordinator X. Suppose $\kappa_1, \kappa_2 > 0$. Following (3.1.2) and the Lévy–Khintchine representation, the Lévy measure of ξ^X is given by

$$v_{\xi^X}(\mathrm{d}z) = v_X\left(\mathrm{d}\frac{z}{\kappa_1}\right) + v_{-X}\left(\mathrm{d}\frac{z}{\kappa_2}\right), \quad z \in \mathbb{R} \setminus \{0\}.$$

Thus, it follows from the inequalities

$$\int_0^1 z^p v_X \left(d \frac{z}{\kappa_1} \right) \le \int_{-1}^1 |z|^p v_{\xi^X}(dz) \le 2 \max \left\{ \int_0^1 z^p v_X \left(d \frac{z}{\kappa_1} \right), \int_0^1 z^p v_X \left(d \frac{z}{\kappa_2} \right) \right\}, \quad p > 0$$

that $\mathfrak{B}(\xi^X) = \mathfrak{B}(X)$, as required. If either κ_1 or κ_2 is zero the result is immediate.

Corollary 5

Proof. The formulae follow immediately by replacing X with its regulated counterparts in (3.2.2).

Corollary 6

Proof. Again, with Corollary 1 we only consider the Gaussian mixture Ξ^X based on X. By construction, the Lévy measure of Ξ^X satisfies

$$v_{\Xi^X}(\mathrm{d}y) = \int_0^\infty v_X(\mathrm{d}s) \gamma_s(\mathrm{d}y), \quad y \in \mathbb{R} \setminus \{0\},$$

where γ_t , for t > 0, represents the Gaussian measure with mean θt and variance t, that is, the probability measure of the drifted Brownian motion $\theta t + W_t$. For every p > 0, by the Fubini–Tonelli theorem we have

$$\int_{-1}^{1} |y|^p \int_{0}^{\infty} v_X(\mathrm{d}s) \gamma_s(\mathrm{d}y) = \int_{0}^{\infty} v_X(\mathrm{d}s) \mathsf{E} \big[|\theta s + \sqrt{s}\zeta|^p \mathbb{1}_{A_s} \big],$$

 ζ being a standard normal random variable and $A_s := \{|\theta s + \sqrt{s}\zeta| \le 1\}$. From the fact that

$$\int_{1}^{\infty} v_X(\mathrm{d}s) \mathsf{E}[|\theta s + \sqrt{s}\zeta|^p \mathbb{1}_{A_s}] \le v_X([1,\infty)) < \infty,$$

the finiteness of $\int_0^\infty v_X(\mathrm{d}s) \mathsf{E}\big[|\theta s + \sqrt{s}\zeta|^p \mathbb{1}_{A_s}\big]$ is the same as that of $\int_0^1 v_X(\mathrm{d}s) \mathsf{E}\big[|\theta s + \sqrt{s}\zeta|^p \mathbb{1}_{A_s}\big]$. Towards that end, we first apply the C^p -inequality to obtain for every $p > 2\mathfrak{B}(X)$

$$\int_{0}^{1} \mathsf{E} \left[|\theta s + \sqrt{s} \zeta|^{p} \mathbb{1}_{A_{s}} \right] v_{X}(\mathrm{d}s) \leq 2^{(p-1)^{+}} \left(\theta^{p} \int_{0}^{1} s^{p} \mathsf{E} \left[\mathbb{1}_{A_{s}} \right] v_{X}(\mathrm{d}s) + \int_{0}^{1} s^{p/2} \mathsf{E} \left[|\zeta|^{p} \mathbb{1}_{A_{s}} \right] v_{X}(\mathrm{d}s) \right) \\
\leq 2^{(p-1)^{+}} \left(\theta^{p} \int_{0}^{1} s^{p} v_{X}(\mathrm{d}s) + \mathsf{E} \left[|\zeta|^{p} \right] \int_{0}^{1} s^{p/2} v_{X}(\mathrm{d}s) \right) \\
\leq \infty.$$

so that $\mathfrak{B}(\Xi^X) \leq 2\mathfrak{B}(X)$. Second, for every $p < 2\mathfrak{B}(X)$, observe that

$$\begin{split} \int_{0}^{1} \mathsf{E} \big[|\theta s + \sqrt{s} \zeta|^{p} \mathbb{I}_{A_{s}} \big] v_{X}(\mathrm{d}s) & \geq \int_{0}^{1} \frac{s^{p/2}}{\sqrt{2\pi}} \int_{\theta \sqrt{s}}^{\theta \sqrt{s} + 1/\sqrt{s}} (x - \theta \sqrt{s})^{p} e^{-z^{2}/2} \mathrm{d}x \, v_{X}(\mathrm{d}s) \\ & = \int_{0}^{1} \frac{s^{p/2}}{\sqrt{2\pi}} \int_{0}^{1/\sqrt{s}} x^{p} \exp \left(-\frac{(x + \theta \sqrt{s})^{2}}{2} \right) \mathrm{d}x \, v_{X}(\mathrm{d}s) \\ & \geq \int_{0}^{1} \frac{s^{p/2}}{\sqrt{2\pi}} \int_{0}^{1} x^{p} \exp \left(-\frac{(x + \theta)^{2}}{2} \right) \mathrm{d}x \, v_{X}(\mathrm{d}s) \\ & = \mathsf{E} \big[(\zeta - \theta)^{p} \mathbb{I}_{[\theta, \theta + 1]}(\zeta) \big] \int_{0}^{1} s^{p/2} v_{X}(\mathrm{d}s) \\ & = \infty, \end{split}$$

where the second equality uses the substitution $x - \theta \sqrt{s} \mapsto x$ and which implies that $\mathfrak{B}(\Xi^X) \ge 2\mathfrak{B}(X)$. It is therefore concluded that $\mathfrak{B}(Z) = 2\mathfrak{B}(X)$, as required.

Proposition 1

Proof. For the type I, plugging the stated LT of X_1 into the first formula in (2.1.5) and applying substitution as in (A.3) the LT of $\bar{X}_1^{(n)}$ reads for n > 0

$$\phi_{\bar{X}_1^{(n)}}(u) = \exp\left(\lambda \left(\int_0^1 e^{-(1-\Gamma(n,-\log s)/\Gamma(n))u} ds - 1 \right) \right)$$

$$= \exp\left(\lambda \left(\Gamma(n) \int_0^1 \frac{e^{-uz}}{Q^{n-1}(n,1-z)} dz - 1 \right) \right), \tag{A.4}$$

which is clearly an entire function.

The general formula for the type II is immediate from the second formula in (2.1.5). If $n \in \mathbb{N}_{++}$, then with $\int_0^1 (-\log v)^{n-1} / \Gamma(n) dv = 1$ we have that

$$\frac{1}{\Gamma(n)} \int_0^1 e^{-uv} (-\log v)^{n-1} dv = \sum_{k=0}^\infty \int_0^1 \frac{(-\log v)^{n-1} (-uv)^k}{\Gamma(n) k!} dv$$

$$= \sum_{k=0}^\infty \frac{(-u)^k}{(k+1)^n k!}$$

$$= \sum_{k=0}^\infty \frac{(-u)^k}{k!} \left(\frac{\prod_{j=1}^k j}{\prod_{j=1}^k (j+1)} \right)^n$$

$$= {}_n F_n(1, \dots, 1; 2 \dots, 2; -u),$$

where the second equality follows from the proof of Corollary 2 and which is also entire.

For the type III, note that

$$\phi_{\check{X}_1^{(n)}}(u) = \exp\left(\lambda \left(\int_0^1 e^{-s^n u/\Gamma(n+1)} \mathrm{d}s - 1\right)\right), \quad u \in \mathbb{C}$$

applies to non-integer values of n as well. The integral can be directly evaluated with the substitution $s^n \mapsto s$, leading to the third formula in (4.1.1).

The formulae (4.1.2) for the Lévy densities are direct consequences of (2.2.2) or (2.2.3) after taking $v(dz) = \lambda \delta_{\{1\}}(dz)$ with the dirac measure.

Proposition 2

Proof. Given $n \in \mathbb{N}_{++}$, starting with the LT of $Y_1^{(n)}$, we have using binomial expansion and the proof of Corollary 2 that for c > 0,

$$\begin{split} \frac{1}{\Gamma(n)} \int_0^1 (-\log v)^{n-1} (uv+b)^c \mathrm{d}v &= \sum_{k=0}^\infty \int_0^1 \binom{c}{k} \frac{b^c (-\log v)^{n-1}}{\Gamma(n)} \left(\frac{uv}{b}\right)^k \mathrm{d}v \\ &= b^c \sum_{k=0}^\infty \binom{c}{k} \frac{(u/b)^k}{(k+1)^n} \\ &= b^c \sum_{k=0}^\infty \frac{1}{k!} \left(\frac{u}{b}\right)^k \frac{(-1)^k (k!)^n \prod_{j=1}^k (j-c-1)}{((k+1)!)^n} \\ &= b^c \ _{n+1} \mathrm{F}_n \Big(1, \dots, 1, -c; 2, \dots, 2; -\frac{u}{b}\Big), \end{split}$$

where in the first equality the interchange of integration and summation for $u \in (D_0(b))^{\complement} \setminus (-\infty, -b]$ is justified by analytic continuation.

The limiting case c = 0 (corresponding to the gamma process) cannot be immediately gleaned from the last result. Similarly, by performing a separate computation we have

$$\frac{1}{\Gamma(n)} \int_{0}^{1} (-\log v)^{n-1} \log \frac{b}{uv + b} dv = \sum_{k=1}^{\infty} \int_{0}^{1} \frac{(-\log v)^{n-1}}{k\Gamma(n)} \left(-\frac{uv}{b}\right)^{k} dv
= \sum_{k=1}^{\infty} \frac{(-u/b)^{k}}{k(k+1)^{n}}
= \sum_{k=1}^{\infty} \left(-\frac{u}{b}\right)^{k} \left(\frac{1}{k} - \sum_{j=1}^{n} (k+1)^{-j}\right)
= n - \left(1 + \frac{b}{u}\right) \log \frac{u+b}{b} + \frac{b}{u} \sum_{j=2}^{n} \text{Li}_{j} \left(-\frac{u}{b}\right).$$

Thus, after some rearrangement we arrive at the first formula in (4.2.1).

Explicit computation of the Lévy density $\tilde{\ell}^{(n)}$ ($n \in \mathbb{N}_{++}$) is subtler because the integral inside (2.2.3) is concentrated on the tail behavior of ν , which obstructs direct expansion. Alternatively, observe that the recurrence relation leading to it, i.e.,

$$\tilde{\ell}^{(n)}(z) = \int_{1}^{\infty} \frac{\tilde{\ell}^{(n-1)}(yz)}{y} dy, \quad z > 0, \tag{A.5}$$

is nothing but an Euler integral equation for the G-function (documented in [Bateman and Erdélyi, 1954, Eq. 20.5.2] [11]), or

$$\int_0^\infty \frac{1}{y} G_{p,q}^{l,m} \begin{pmatrix} \alpha_1, \dots, \alpha_p \\ \beta_1, \dots, \beta_q \end{pmatrix} w y dy = G_{p+1,q+1}^{l+1,m} \begin{pmatrix} \alpha_1, \dots, \alpha_p, 1 \\ 0, \beta_1, \dots, \beta_q \end{pmatrix} w$$

to be precise, where $0 \le m \le p$ and $0 \le l \le q$ are all integers and $w \equiv w(z) > 0$ is linear. By employing an induction argument the general solution to (A.5) reads

$$\tilde{\ell}^{(n)}(z) = dG_{p+n,q+n}^{l+n,m} \left(\begin{array}{c} \alpha_1, \dots, \alpha_p, \overbrace{1, \dots, 1}^n \\ \underbrace{0, \dots, 0}_n, \beta_1, \dots, \beta_q \end{array} \middle| w \right), \quad n \in \mathbb{N},$$

for some yet-to-be-determined numbers $m, l, p, q \in \mathbb{N}$ and d > 0. Given the initial condition that $\tilde{\ell}^{(0)}(z) = ae^{-bz}/z^{c+1}$, z > 0, we are forced to choose m = p = 0 and l = q = 1, with $\beta_1 = -c - 1$, in which case the G-function specializes for n = 0 to

$$G_{0,1}^{1,0}\left(\begin{array}{c|c} -c-1 & w \end{array}\right) = \frac{e^{-w}}{w^{c+1}},$$

from where it remains to set w = bz and $d = ab^{c+1}$.

The formulae for the type III are easily obtained by adapting the binomial expansion argument used for the type II. \Box

Proposition 3

Proof. Let X be a Poisson process and consider its constant mixture plus an independent Brownian motion. From Subsection 3.1 and Subsection 4.1 we know that the model cumulants (with regulation degrees) over the time period of Δ are given by

$$\begin{split} K_{\Delta}^{(n)}(1) &= \Delta \Big(\mu_n - \rho(1,n) \frac{\lambda_n}{b_n} \Big), \quad K_{\Delta}^{(n)}(2) &= \Delta \Big(\sigma_n^2 + \rho(2,n) \frac{\lambda_n}{b_n^2} \Big), \\ K_{\Delta}^{(n)}(3) &= -\Delta \rho(3,n) \frac{\lambda_n}{b_n^3}, \quad K_{\Delta}^{(n)}(4) &= \Delta \rho(4,n) \frac{\lambda_n}{b_n^4}, \quad n \in \mathfrak{N}, \end{split}$$

where recall that $\mathfrak{N} \subsetneq \mathbb{R}_+$ is the truncated and discretized n-domain for experimentation, and $\rho(m, n)$'s are specified in (5.1.1). We then immediately have the following quotient relation:

$$\frac{K_{\Delta}^{(n)}(4)}{K_{\Delta}^{(n)}(3)} = -\frac{\rho(4,n)}{\rho(3,n)} \frac{1}{b_n},$$

which combined with the four moment conditions in (5.1.2) pins down the rate parameter estimate \hat{b}_n , and subsequently the other estimates in (5.1.3).

Proposition 4

Proof. Consider the case of the Gaussian mixture of *X* being a tempered stable subordinator. Using the results obtained in Subsection 3.2 and Subsection 4.2 we have the following model cumulants:

$$\begin{split} K_{\Delta}^{(n)}(1) &= \Delta(\mu_n + \theta_n \rho(1, n) K_{n;\Delta}(1)), \\ K_{\Delta}^{(n)}(2) &= \Delta(\rho(1, n) K_{n;\Delta}(1) + \theta_n^2 \rho(2, n) K_{n;\Delta}(2)), \\ K_{\Delta}^{(n)}(3) &= \Delta(3\theta_n \rho(2, n) K_{n;\Delta}(2) + \theta_n^3 \rho(3, n) K_{n;\Delta}(3)), \\ K_{\Delta}^{(n)}(4) &= \Delta(3\rho(2, n) K_{n;\Delta}(2) + 6\theta_n^2 \rho(3, n) K_{n;\Delta}(3) + \theta_n^4 \rho(4, n) K_{n;\Delta}(4)), \end{split}$$

where

$$K_{n;\Delta}(1) = \Gamma(1-c) \frac{a_n}{b_n^{1-c}}, \quad K_{n;\Delta}(2) = \frac{1-c}{b_n} K_{n;\Delta}(1),$$

$$K_{n;\Delta}(3) = \frac{(2-c)(1-c)}{b_n^2} K_{n;\Delta}(1), \quad K_{n;\Delta}(4) = \frac{(3-c)(2-c)(1-c)}{b_n^3} K_{n;\Delta}(1)$$

are the first four cumulants of X_{Δ} with regulation degree-subscripted parameters. From here one can deduce the following cumulant quotient relations:

$$\begin{split} \frac{K_{\Delta}^{(n)}(3)}{K_{\Delta}^{(n)}(2)} &= \theta_n (1-c) \Big(3 \frac{\rho(2,n)}{\rho(1,n)} + \theta_n^2 \frac{\rho(3,n)}{\rho(1,n)} \frac{(2-c)}{b_n} \Big) \Big(b_n + \theta_n^2 \frac{\rho(2,n)}{\rho(1,n)} (1-c) \Big)^{-1}, \\ \frac{K_{\Delta}^{(n)}(4)}{K_{\Delta}^{(n)}(2)} &= (1-c) \Big(3 \frac{\rho(2,n)}{\rho(1,n)} + 6 \theta_n^2 \frac{\rho(3,n)}{\rho(1,n)} \frac{2-c}{b_n} + \theta_n^4 \frac{\rho(4,n)}{\rho(1,n)} \frac{(3-c)(2-c)}{b_n^2} \Big) \Big(b_n + \theta_n^2 \frac{\rho(2,n)}{\rho(1,n)} (1-c) \Big)^{-1}, \end{split}$$

which define a rational system for b_n and θ_n . Note that the latter two conditions in (5.1.2) can be equivalently written as $K_{\Delta}^{(n)}(3)/K_{\Delta}^{(n)}(2) = [SK][V]^{1/2}$ and $K_{\Delta}^{(n)}(4)/K_{\Delta}^{(n)}(2) = [EK][V]$; from the first condition the sign of θ_n is seen to be determined by that of [SK], and then using the second the equation (5.1.5) governing its absolute value $|\theta_n|$ can be easily derived. Notice that, as long as the condition

$$\frac{3-c}{2-c}\frac{\rho(4,n)\rho(2,n)}{\rho(3,n)^2} < \frac{[EK]}{[SK]^2}$$

is fulfilled, a real solution of (5.1.5) always exists and can be easily located numerically; otherwise, the equation may not admit a real solution. Upon rearranging terms we obtain the estimates in (5.1.4) as desired.

Appendix B Alternative skewness and excess kurtosis enlargement for tempered stable subordinators

For each $n \in \mathbb{N}$ (including zero), let X_n be a tempered stable subordinator with parametrization $\{a_n > 0, b_n > 0, c \in [0, 1)\}$, and $X_0 \equiv X$ ($a_0 = a$ and $b_0 = b$). We know from [Küchler and Tappe, 2013, Eq. 2.19] [41] that the mean and variance at fixed t > 0 are respectively

$$\mathsf{E} X_{n,t} = rac{\Gamma(1-c) \, a_n \, t}{b_n^{1-c}}, \quad \mathsf{Var} X_{n,t} = rac{\Gamma(2-c) \, a_n \, t}{b_n^{2-c}}.$$

We stick to writing $\# \in \{X, Y, Z\}$ as a placeholder for any type of regulated stochastic clocks, whose mth cumulant is $\rho(m, n) \in (0, 1]$ times that of X_t (see (5.1.1)). Then, from the quotient relation $\text{Var}X_{n,t}/\text{E}X_{n,t} = (1-c)/b_n$ and the first two formulae in (2.3.3), (2.3.5), and (2.3.6) we have

$$\frac{\mathsf{Var#}_t^{(n)}}{\mathsf{E#}_t^{(n)}} = \frac{(1-c)\rho(2,n)}{b_n\rho(1,n)}.$$

Following $\#^{(n)}$ is understood to be X_n -clocks with parameters a_n , b_n , and c, as opposed to X-clocks. If we keep the mean and variance of $\#^{(n)}_t$ to be invariant across $n \ge 1$, we need

$$a_n = \frac{\rho^{1-c}(2,n)}{\rho^{2-c}(1,n)}a, \quad b_n = \frac{\rho(2,n)}{\rho(1,n)}b.$$

It then follows that

$$\mathsf{Skew} X_{n,t} = \frac{\Gamma(3-c) a_n / b_n^{3-c}}{(\Gamma(2-c) a_n / b_n^{2-c})^{3/2}} = \frac{2-c}{\Gamma(2-c)^{1/2} a_n^{1/2} b_n^{c/2}} = \frac{\rho(1,n)}{\rho^{1/2}(2,n)} \mathsf{Skew} X_t,$$

$$\mathsf{EKurt} X_{n,t} = \frac{\Gamma(4-c) \, a_n / b_n^{4-c}}{(\Gamma(2-c) \, a_n / b_n^{2-c})^2} = \frac{(3-c)(2-c)}{\Gamma(2-c) \, a_n b_n^c} = \frac{\rho^2(1,n)}{\rho(2,n)} \mathsf{EKurt} X_t.$$

Therefore, according to the last two formulae in (2.3.3), (2.3.5), and (2.3.6) we obtain for any $n \in \mathbb{N}$

$$\mathsf{Skew}\#_t^{(n)} = \frac{\rho(1,n)\rho(3,n)}{\rho^2(2,n)} \mathsf{Skew}X_t, \quad \mathsf{EKurt}\#_t^{(n)} = \frac{\rho^2(1,n)\rho(4,n)}{\rho^3(2,n)} \mathsf{EKurt}X_t, \quad t > 0,$$

which as well apply to any non-integer values of n > 0. Specifying the last results for $\rho(m, n)$ according to (5.1.1) delivers the results.